Model–Independent Determination of the WIMP Mass from Direct Dark Matter Detection Data

Manuel Drees[1,2] and Chung-Lin Shan[1]

[1] *Physikalisches Inst. der Univ. Bonn, Nussallee 12, 53115 Bonn, Germany*
[2] *KIAS, School of Physics, 207–43 Cheongnyangni–dong, Seoul 130–012, Republic of Korea*

Abstract

Weakly Interacting Massive Particles (WIMPs) are one of the leading candidates for Dark Matter. We develop a model–independent method for determining the mass m_χ of the WIMP by using data (i.e., measured recoil energies) of direct detection experiments. Our method is independent of the as yet unknown WIMP density near the Earth, of the form of the WIMP velocity distribution, as well as of the WIMP–nucleus cross section. However, it requires positive signals from at least two detectors with different target nuclei. In a background–free environment, $m_\chi \sim 50$ GeV could in principle be determined with an error of $\sim 35\%$ with only 2×50 events; in practice upper and lower limits on the recoil energy of signal events, imposed to reduce backgrounds, can increase the error. The method also loses precision if m_χ significantly exceeds the mass of the heaviest target nucleus used.

arXiv:0803.4477v3 [hep-ph] 17 Jun 2008

1 Introduction

First indications for the existence of Dark Matter were already found in the 1930s [1]. By now there is strong evidence [1]-[5] to believe that a large fraction (more than 80%) of all matter in the Universe is dark (i.e., interacts at most very weakly with electromagnetic radiation and ordinary matter). The dominant component of this cosmological Dark Matter must be due to some yet to be discovered, non–baryonic particles. Weakly Interacting Massive Particles (WIMPs) χ are one of the leading candidates for Dark Matter. WIMPs are stable particles which arise in several extensions of the Standard Model of electroweak interactions. Typically they are presumed to have masses between 10 GeV and a few TeV and interact with ordinary matter only weakly (for reviews, see [6]).

Currently, the most promising method to detect many different WIMP candidates is the direct detection of the recoil energy deposited in a low–background laboratory detector by elastic scattering of ambient WIMPs on the target nuclei [7, 8]. The recoil energy spectrum can be calculated from an integral over the one–dimensional WIMP velocity distribution $f_1(v)$, where v is the absolute value of the WIMP velocity in the laboratory frame. If this function is known, the WIMP mass m_χ can be obtained from a one–parameter fit to the normalized recoil spectrum [9], once a positive WIMP signal has been found. However, this introduces a systematic uncertainty which is difficult to control. We remind the reader that $N-$body simulations of the spatial distribution of Cold Dark Matter (which includes WIMPs) seem to be at odds with observations at least in the central region of galaxies [10]; this may have ramifications for f_1 as well. On the theory side, several modifications of the standard "shifted Maxwellian" distribution [6] have been suggested, ranging from co– or counter–rotating halos [11] to scenarios where the three–dimensional WIMP velocity distribution gets large contributions from discrete "streams" with (nearly) fixed velocity [12, 13].

The goal of our work is to develop model–independent methods which allow to determine m_χ directly from (future) experimental data. This builds on our earlier work [14], where we showed how to determine (moments of) $f_1(v)$ from the recoil spectrum in direct WIMP detection experiments. In this earlier analysis m_χ had been the only input required; one does not need to know the WIMP–nucleus scattering cross section, nor the local WIMP density. The fact that this method will give a result for f_1 for any assumed value of m_χ already tells us that one will need at least two different experiments, with different target nuclei, to model–independently determine the WIMP mass from direct detection experiments. To do so, one simply requires that the values of a given moment of f_1 determined by both experiments agree. This leads to a simple expression for m_χ, which can easily be solved analytically; note that each moment can be used. An additional expression for m_χ can be derived under the assumption that the ratio of scattering cross sections on protons and neutrons is known. This is true e.g., for spin–independent scattering of a supersymmetric neutralino, which is the perhaps best motivated WIMP candidate [6]; in this case the spin–independent cross section for scattering on a proton is almost the same as that for scattering on a neutron. Not surprisingly, the best result obtains by combining measurements of several moments with that derived from the assumption about the ratio of cross sections.

The remainder of this article is organized as follows. In Sec. 2 we review briefly the methods for estimating the moments of the velocity distribution function, paying special attention to experimentally imposed limits on the range of allowed recoil energies. In Sec. 3 we will present the formalism for determining the WIMP mass. Numerical results, based on Monte Carlo simulations of future experiments, will be presented in Sec. 4. We conclude in Sec. 5. Some technical details of our calculation will be given in an Appendix.

2 Determining the moments of the velocity distribution of WIMPs

In this section we review briefly the method for estimating the moments of the one–dimensional velocity distribution function f_1 of WIMPs from the elastic WIMP–nucleus scattering data. We first discuss the formalism, and then describe how it can be implemented directly using (simulated, or future real) data from direct WIMP search experiments.

2.1 Formalism

Our analysis starts from the basic expression for the differential rate for elastic WIMP–nucleus scattering [6]:

$$\frac{dR}{dQ} = \mathcal{A} F^2(Q) \int_{v_{\min}}^{\infty} \left[\frac{f_1(v)}{v} \right] dv. \tag{1}$$

Here R is the direct detection event rate, i.e., the number of events per unit time and unit mass of detector material, Q is the energy deposited in the detector, $F(Q)$ is the elastic nuclear form factor, and v is the absolute value of the WIMP velocity in the laboratory frame. The constant coefficient $\mathcal{A}$ is defined as

$$\mathcal{A} \equiv \frac{\rho_0 \sigma_0}{2 m_\chi m_{\mathrm{r,N}}^2}, \tag{2}$$

where ρ_0 is the WIMP density near the Earth and σ_0 is the total cross section ignoring the form factor suppression. The reduced mass $m_{\mathrm{r,N}}$ is defined as

$$m_{\mathrm{r,N}} \equiv \frac{m_\chi m_{\mathrm{N}}}{m_\chi + m_{\mathrm{N}}}, \tag{3}$$

where m_χ is the WIMP mass and m_{N} that of the target nucleus. Finally, $v_{\min}$ is the minimal incoming velocity of incident WIMPs that can deposit the energy Q in the detector:

$$v_{\min} = \alpha \sqrt{Q}, \tag{4}$$

where we define

$$\alpha \equiv \sqrt{\frac{m_{\mathrm{N}}}{2 m_{\mathrm{r,N}}^2}}. \tag{5}$$

Eq.(1) can be solved for f_1 [14]:

$$f_1(v) = \mathcal{N} \left\{ -2Q \cdot \frac{d}{dQ} \left[\frac{1}{F^2(Q)} \left(\frac{dR}{dQ} \right) \right] \right\}_{Q=v^2/\alpha^2}, \tag{6}$$

where the normalization constant $\mathcal{N}$ is given by

$$\mathcal{N} = \frac{2}{\alpha} \left\{ \int_0^{\infty} \frac{1}{\sqrt{Q}} \left[\frac{1}{F^2(Q)} \left(\frac{dR}{dQ} \right) \right] dQ \right\}^{-1}. \tag{7}$$

Note that, first, because $f_1(v)$ in Eq.(6) is the *normalized* velocity distribution, the normalization constant $\mathcal{N}$ here is *independent* of the constant coefficient $\mathcal{A}$ defined in Eq.(2). Second, the integral here goes over the entire physically allowed range of recoil energies, starting at $Q = 0$. The upper limit of the integral has been written as ∞. However, it is usually assumed that the

WIMP flux on Earth is negligible at velocities exceeding the escape velocity $v_{esc} \simeq 700$ km/s. This leads to a kinematic maximum of the recoil energy,

$$Q_{\max,\mathrm{kin}} = \frac{v_{esc}^2}{\alpha^2} \, , \tag{8}$$

where α has been given in Eq.(5). Eq.(7) then implies

$$\int_0^\infty f_1(v) \, dv = \int_0^{v_{esc}} f_1(v) \, dv = 1 \, . \tag{9}$$

Using Eq.(6), the moments of f_1 can be expressed as [14]

$$\langle v^n \rangle = \int_0^{v_{esc}} v^n f_1(v) \, dv = \mathcal{N} \left(\frac{\alpha^{n+1}}{2} \right) (n+1) I_n \, , \tag{10}$$

which holds for all $n \geq 0$. Here the integral I_n is given by

$$I_n = \int_0^{Q_{\max,\mathrm{kin}}} Q^{(n-1)/2} \left[\frac{1}{F^2(Q)} \left(\frac{dR}{dQ} \right) \right] dQ \, . \tag{11}$$

In this notation, Eq.(7) can be re–written as $\mathcal{N} = 2/(\alpha I_0)$.

The results in Eqs.(6) and (10) depend on the WIMP mass m_χ only through the coefficient α defined in Eq.(5). Evidently any (assumed) value of m_χ will lead to a well–defined, normalized distribution function f_1 when used in Eq.(6). Hence m_χ can be extracted from a *single* recoil spectrum *only if* one makes some assumptions about the velocity distribution $f_1(v)$.

A model–independent determination of m_χ thus requires that at least two different recoil spectra, with two different target nuclei, have been measured. As we will show in detail in the next section, m_χ can then be obtained from the requirement that these two spectra lead to the same moments of f_1.

Before coming to that, we have to incorporate the effects of a finite energy acceptance of the detector. Any real detector will have a certain threshold energy Q_{thre} below which it cannot register events. Off–line one may need to impose a cut $Q > Q_{\min} > Q_{\mathrm{thre}}$ in order to suppress (instrumental or physical) backgrounds. Similarly, background rejection may require a maximum energy cut, $Q < Q_{\max} \leq Q_{\max,\mathrm{kin}}$. In fact, we will see below that, at least for smallish data samples, such a cut might even be beneficial for the determination of m_χ. We therefore now give expressions for the case that only data with $Q_{\min} \leq Q \leq Q_{\max}$ are used in the analysis.

To that end, we introduce generalized moments of f_1:

$$\langle v^n \rangle (v_1, v_2) = \int_{v_1}^{v_2} v^n f_1(v) \, dv$$
$$= \mathcal{N} \alpha^{n+1} \left[\frac{Q_1^{(n+1)/2} r(Q_1)}{F^2(Q_1)} - \frac{Q_2^{(n+1)/2} r(Q_2)}{F^2(Q_2)} + \left(\frac{n+1}{2} \right) I_n(Q_1, Q_2) \right] \, , \tag{12}$$

where we have introduced the short–hand notation

$$r(Q_i) = \left. \frac{dR}{dQ} \right|_{Q=Q_i} \, , \qquad\qquad i = 1, \, 2 \, , \tag{13}$$

and

$$I_n(Q_1, Q_2) = \int_{Q_1}^{Q_2} Q^{(n-1)/2} \left[\frac{1}{F^2(Q)} \left(\frac{dR}{dQ} \right) \right] dQ \, . \tag{14}$$

In order to arrive at the final expression in Eq.(12) we used Eq.(6) and integrated by parts. The Q_i in Eqs.(12)–(14) are related to the original integration limits v_i appearing on the left–hand side of Eq.(12) via Eq.(4), i.e.,

$$Q_i = \frac{v_i^2}{\alpha^2}, \qquad\qquad i = 1,\ 2. \qquad\qquad (15)$$

Of course, Eq.(12) reduces to Eq.(10) in the limit $v_1 \to 0$, $v_2 \to v_{\rm esc}$; note, however, that Eq.(12) is also applicable for the case $n = -1$, where the last term on the right–hand side vanishes. The same restriction on the WIMP velocity can also be introduced in the normalization constant $\mathcal{N}$ of Eq.(7), in which case $\int_{v_1}^{v_2} f_1(v)\,dv$ is normalized to unity. Formally this can be treated using Eqs.(12)–(15) by demanding $\langle v^0 \rangle (v_1, v_2) = 1$.

2.2   Experimental implementation

In order to directly use our results for $f_1(v)$ and for its moments $\langle v^n \rangle$ given in Eqs.(6), (10) and (12), one needs a functional form for the recoil spectrum dR/dQ. In practice this results usually from a fit to experimental data. However, data fitting can re–introduce some model dependence and makes the error analysis more complicated. Hence, expressions that allow to reconstruct $f_1(v)$ and its moments directly from the data have been developed [14]. We started by considering experimental data described by

$$Q_n - \tfrac{b_n}{2} \le Q_{n,i} \le Q_n + \tfrac{b_n}{2}, \qquad\qquad i = 1,\ 2,\ \cdots,\ N_n,\ n = 1,\ 2,\ \cdots,\ B. \qquad (16)$$

Here the total energy range has been divided into B bins with central points Q_n and widths b_n. In each bin, N_n events will be recorded. Note that we assume that the sample to be analyzed only contains signal events, i.e., is free of background, and ignore the uncertainty on the measurement of the recoil energy Q. Active background suppression techniques [15] should make the former possible. The energy resolution of most existing detectors is so good that its error will be negligible compared to the statistical uncertainty for the foreseeable future.

Since the recoil spectrum dR/dQ is expected to be approximately exponential, we used the following ansatz for the spectrum in the n−th bin [14]:

$$\left(\frac{dR}{dQ}\right)_n \equiv \left(\frac{dR}{dQ}\right)_{Q \simeq Q_n} \simeq \widetilde{r}_n\, e^{k_n(Q - Q_n)} \equiv r_n\, e^{k_n(Q - Q_{s,n})}. \qquad (17)$$

Here r_n is the standard estimator for dR/dQ at $Q = Q_n$,

$$r_n = \frac{N_n}{b_n}, \qquad\qquad (18)$$

$\widetilde{r}_n$ is the value of the recoil spectrum at the point $Q = Q_n$,

$$\widetilde{r}_n \equiv \left(\frac{dR}{dQ}\right)_{Q = Q_n} = r_n \left[\frac{k_n b_n/2}{\sinh(k_n b_n/2)}\right], \qquad\qquad (19)$$

and k_n is the logarithmic slope of the recoil spectrum in the n−th bin. It can be computed numerically from the average Q−value in the n−th bin:

$$\overline{Q - Q_n}\big|_n = \left(\frac{b_n}{2}\right) \coth\left(\frac{k_n b_n}{2}\right) - \frac{1}{k_n}, \qquad\qquad (20)$$

where

$$\overline{(Q - Q_n)^\lambda}|_n \equiv \frac{1}{N_n} \sum_{i=1}^{N_n} (Q_{n,i} - Q_n)^\lambda .$$ (21)

Finally, $Q_{s,n}$ is the shifted point at which the leading systematic error due to the ansatz in Eq.(17) is minimal [14],

$$Q_{s,n} = Q_n + \frac{1}{k_n} \ln \left[\frac{\sinh(k_n b_n / 2)}{k_n b_n / 2} \right] .$$ (22)

Note that $Q_{s,n}$ differs from the central point of the $n-$th bin, Q_n.

Using Eqs.(12) and (13) with $Q_1 = Q_{\min}$ and $Q_2 = Q_{\max}$, the generalized $n-$th moment of the velocity distribution function can be written as

$$\langle v^n \rangle (v(Q_{\min}), v(Q_{\max})) = \alpha^n \left[\frac{2Q_{\min}^{(n+1)/2} r(Q_{\min}) / F^2(Q_{\min}) + (n+1) I_n(Q_{\min}, Q_{\max})}{2Q_{\min}^{1/2} r(Q_{\min}) / F^2(Q_{\min}) + I_0(Q_{\min}, Q_{\max})} \right] ,$$ (23)

where $v(Q) = \alpha\sqrt{Q}$. Here we have implicitly assumed that $Q_{\max}$ is so large that terms $\propto r(Q_{\max})$ are negligible. We will see later that this is not necessarily true for $n \geq 1$, since these moments receive sizable contributions from large recoil energies [14]. Nevertheless we will show in Sec. 3 that even in that case, Eq.(23) can still be used for determining m_χ. From the ansatz Eq.(17), the counting rate at $Q_{\min}$ can be expressed as

$$r(Q_{\min}) = r_1 e^{k_1(Q_{\min} - Q_{s,1})} .$$ (24)

The integral $I_n(Q_{\min}, Q_{\max})$ defined in Eq.(14) can be estimated through the sum:

$$I_n(Q_{\min}, Q_{\max}) = \sum_a \frac{Q_a^{(n-1)/2}}{F^2(Q_a)} ,$$ (25)

where the sum runs over all events in the data set that satisfy $Q_a \in [Q_{\min}, Q_{\max}]$.

Since all I_n are determined from the same data, they are correlated, with [14]

$$\text{cov}(I_n, I_m) = \sum_a \frac{Q_a^{(n+m-2)/2}}{F^4(Q_a)} ,$$ (26)

where the sum again runs over all events with recoil energy between $Q_{\min}$ and $Q_{\max}$.

On the other hand, the statistical error of $r(Q_{\min})$ can be obtained from Eq.(24) as

$$\sigma^2(r(Q_{\min})) = r^2(Q_{\min}) \left\{ \frac{\sigma^2(r_1)}{r_1^2} + \left[\frac{1}{k_1} - \left(\frac{b_1}{2} \right) \left(1 + \coth \left(\frac{b_1 k_1}{2} \right) \right) \right]^2 \sigma^2(k_1) \right\} .$$ (27)

The error on r_1 follows directly from its definition in Eq.(18):

$$\sigma^2(r_n) = \frac{N_n}{b_n^2} .$$ (28)

The error on the logarithmic slope k_1 can be computed from Eq.(20):

$$\sigma^2(k_n) = k_n^2 \left\{ 1 - \left[\frac{k_n b_n / 2}{\sinh(k_n b_n / 2)} \right]^2 \right\}^{-1} \sigma^2 \left(\overline{Q - Q_n}|_n \right) ,$$ (29)

with

$$\sigma^2\left(\overline{Q-Q_n}|_n\right) = \frac{1}{N_n-1}\left[\overline{(Q-Q_n)^2}|_n - \overline{Q-Q_n}|_n^2\right]. \tag{30}$$

Finally, the correlation between the errors on $r(Q_{\min})$, which is calculated entirely from the events in the first bin, and on I_n is given by [14]

$$
\begin{aligned}
\text{cov}&(r(Q_{\min}), I_n) \\
&= r(Q_{\min})\, I_n(Q_{\min}, Q_{\min}+b_1) \\
&\quad \times \left\{ \frac{\sigma^2(r_1)}{r_1^2} + \left[\frac{1}{k_1} - \left(\frac{b_1}{2}\right)\left(1 + \coth\left(\frac{b_1 k_1}{2}\right)\right)\right] \right. \\
&\qquad\quad \left. \times \left[\frac{I_{n+2}(Q_{\min}, Q_{\min}+b_1)}{I_n(Q_{\min}, Q_{\min}+b_1)} - Q_1 + \frac{1}{k_1} - \left(\frac{b_1}{2}\right)\coth\left(\frac{b_1 k_1}{2}\right)\right] \sigma^2(k_1) \right\} ; \tag{31}
\end{aligned}
$$

note that the integrals I_i in Eq.(31) only extend over the first bin, which ends at $Q = Q_{\min}+b_1$.

3   Determining the WIMP mass

We are now ready to describe methods to extract the WIMP mass m_χ from direct detection data. Recall that m_χ is an *input* in the determination of f_1 and its moments as described in the previous section. In particular, m_χ appears in the factor α^n on the right–hand side of Eq.(23) describing the experimental estimate of the moments of f_1. A truly model–independent determination of m_χ from these data will therefore only be possible by requiring that two (or more) experiments, using different target nuclei, lead to the same result for f_1.

Here we focus on the moments of the distribution function, rather than the function itself, since non–trivial information about the former can already be obtained with $\mathcal{O}(20)$ events [14]. We will also show how m_χ can be estimated from the knowledge of the integral I_0 appearing in the normalization of f_1, if the ratio of WIMP scattering cross sections on protons and neutrons is known. For greater clarity, we will first discuss the idealized situation where all signal events, irrespective of their recoil energy Q_a, are included. In the second subsection we will introduce upper and lower limits on Q_a. A third subsection is devoted to a discussion how the different estimators for the WIMP mass can be combined using a χ^2 fit.

3.1   Without cuts on the recoil energy

If no cuts on the recoil energy need to be applied, we can use the original moments, or equivalently, the generalized moments with $v_1 \to 0$ and $v_2 \to v_{\text{esc}}$; recall that the latter is the same as allowing $v_2 \to \infty$, since by assumption $f_1(v) = 0$ for $v > v_{\text{esc}}$. Eq.(23) then simplifies to

$$\langle v^n \rangle = \alpha^n(n+1)\left(\frac{I_n}{I_0}\right), \tag{32}$$

where I_n and I_0 can be estimated as in Eq.(25) with $Q_{\min} \to 0$ and $Q_{\max} \to \infty$ (or, equivalently, $Q_{\max} \to Q_{\max,\text{kin}}$).

Suppose X and Y are two target nuclei. We denote their masses by m_X, m_Y, and their form factors as $F_X(Q)$, $F_Y(Q)$. Similarly, we define $\alpha_{X,Y}$ as in Eq.(5), with $m_N \to m_{X,Y}$. Eq.(32) then implies

$$\alpha_X^n\left(\frac{I_{n,X}}{I_{0,X}}\right) = \alpha_Y^n\left(\frac{I_{n,Y}}{I_{0,Y}}\right). \tag{33}$$

Note that the form factors in the estimates of $I_{n,X}$ and $I_{n,Y}$ using Eq.(25) are different. Eq.(33) can be solved for m_χ using Eqs.(5) and (3):

$$m_\chi = \frac{\sqrt{m_X m_Y} - m_X \mathcal{R}_n}{\mathcal{R}_n - \sqrt{m_X/m_Y}}, \tag{34}$$

where we have defined

$$\mathcal{R}_n \equiv \frac{\alpha_Y}{\alpha_X} = \left(\frac{I_{n,X}}{I_{0,X}} \cdot \frac{I_{0,Y}}{I_{n,Y}}\right)^{1/n}, \qquad n \neq 0, \ -1. \tag{35}$$

Using standard Gaussian error propagation, the statistical error on m_χ estimated from Eq.(34) is

$$\begin{aligned}
\sigma(m_\chi)|_{\langle v^n \rangle} &= \frac{\sqrt{m_X/m_Y}\,|m_X - m_Y|}{\left(\mathcal{R}_n - \sqrt{m_X/m_Y}\right)^2} \cdot \sigma(\mathcal{R}_n) \\
&= \frac{\mathcal{R}_n \sqrt{m_X/m_Y}\,|m_X - m_Y|}{\left(\mathcal{R}_n - \sqrt{m_X/m_Y}\right)^2} \\
&\quad \times \frac{1}{|n|} \left[\frac{\sigma^2(I_{n,X})}{I_{n,X}^2} + \frac{\sigma^2(I_{0,X})}{I_{0,X}^2} - \frac{2\mathrm{cov}(I_{0,X}, I_{n,X})}{I_{0,X} I_{n,X}} + (X \longrightarrow Y)\right]^{1/2}, \tag{36}
\end{aligned}$$

where $\sigma^2(I_{n,X}) = \mathrm{cov}(I_{n,X}, I_{n,X})$ and $\mathrm{cov}(I_{0,X}, I_{n,X})$ and so on can be estimated from Eq.(26).

A second method for determining m_χ starts directly from Eq.(1), plus an assumption about the relative strength for WIMP scattering on protons p and neutrons n. The simplest such assumption is that the scattering cross section is the same for both nucleons. This is in fact an excellent approximation for the spin–independent contribution to the cross section of super-symmetric neutralinos [6], and for all WIMPs which interact primarily through Higgs exchange. Writing the "pointlike" cross section σ_0 of Eq.(2) as

$$\sigma_0 = \left(\frac{4}{\pi}\right) m_{\mathrm{r,N}}^2 A^2 |f_{\mathrm{p}}|^2, \tag{37}$$

where f_{p} is the effective $\chi\chi$pp 4–point coupling, $m_{\mathrm{r,N}}$ is the reduced mass defined in Eq.(3) and A is the number of nucleons in the nucleus, we have from Eqs.(1), (2) and the first Eq.(12):

$$r(Q_{\mathrm{min}}) = \frac{\rho_0}{2m_\chi}\left(\frac{4}{\pi}\right) A^2 |f_{\mathrm{p}}|^2 F^2(Q_{\mathrm{min}}) \langle v^{-1} \rangle (v(Q_{\mathrm{min}}), v_{\mathrm{esc}}). \tag{38}$$

Using the second Eq.(12) we see that the counting rate at Q_{min} in fact drops out, and we are left with

$$1 = \frac{4\sqrt{2}}{\pi}\left(\frac{\mathcal{E}\rho_0 A^2 |f_{\mathrm{p}}|^2}{I_0}\right)\left(\frac{m_{\mathrm{r,N}}}{m_\chi \sqrt{m_{\mathrm{N}}}}\right), \tag{39}$$

where we have assumed $Q_{\mathrm{min}} = 0$. Recall that the rate dR/dQ is defined as rate per unit mass and observation time interval, i.e., we need to divide the actual event rate by the exposure $\mathcal{E} = M\tau$, where M is the (fiducial) mass of the detector and τ the observation time. In our previous discussion this factor always dropped out in the end, due to the appearance of the normalization $\mathcal{N}$. This is true also for the right–hand side of Eq.(38), but not for the $1/\mathcal{E}$ factor on the left–hand side of this equation; hence a factor $\mathcal{E}$ appears in the numerator of Eq.(39).

Note that $\mathcal{E}$ is dimensionless in natural units. On the other hand, the unknown factor $\rho_0 |f_{\mathrm{p}}|^2$ appearing in Eq.(39) will cancel out when we use this identity for two different targets X and Y, leading to the final result

$$m_\chi = \frac{(m_X/m_Y)^{5/2} \, m_Y - m_X \mathcal{R}_\sigma}{\mathcal{R}_\sigma - (m_X/m_Y)^{5/2}} \, . \tag{40}$$

Here we have assumed $m_{X,Y} \propto A_{X,Y}$, and introduced the quantity

$$\mathcal{R}_\sigma = \frac{\mathcal{E}_Y}{\mathcal{E}_X} \left(\frac{I_{0,X}}{I_{0,Y}} \right) \, . \tag{41}$$

Recall that, even though the derivation started from the expression for the counting rate at $Q_{\min}$, this rate actually dropped out when going from Eq.(38) to Eq.(39). The final expression only depends on the quantity $\mathcal{R}_\sigma$, which is estimated from *all* the events in both samples using Eq.(25). The error on m_χ computed from Eq.(40) is therefore comparable to that for m_χ derived from a moment of f_1. Still keeping $Q_{\min} = 0$, we have

$$\sigma(m_\chi)|_\sigma = \frac{\mathcal{R}_\sigma \, (m_X/m_Y)^{5/2} \, |m_X - m_Y|}{\left[\mathcal{R}_\sigma - (m_X/m_Y)^{5/2} \right]^2} \left[\frac{\sigma^2 \, (I_{0,X})}{I_{0,X}^2} + \frac{\sigma^2 \, (I_{0,Y})}{I_{0,Y}^2} \right]^{1/2} \, . \tag{42}$$

Ultimately the $\mathcal{R}_n$, $\mathcal{R}_\sigma$ and the errors in Eqs.(36) and (42) should be estimated from the data directly. In the meantime it is instructive to note that the final expressions for the statistical errors of our estimators for m_χ decompose into two factors. The expectation value of the first factor does not depend on f_1; it can be computed entirely from the masses of the involved particles:

$$\frac{\mathcal{R}_n \sqrt{m_X/m_Y} \, |m_X - m_Y|}{\left(\mathcal{R}_n - \sqrt{m_X/m_Y} \right)^2} = \frac{\mathcal{R}_\sigma \, (m_X/m_Y)^{5/2} \, |m_X - m_Y|}{\left[\mathcal{R}_\sigma - (m_X/m_Y)^{5/2} \right]^2}$$

$$= \frac{(m_\chi + m_X) \, (m_\chi + m_Y)}{|m_X - m_Y|}$$

$$\equiv \kappa \, . \tag{43}$$

Here we have made use of the identities $\mathcal{R}_n = \alpha_Y/\alpha_X$ in Eq.(35) and

$$\mathcal{R}_\sigma = \left(\frac{m_X}{m_Y} \right)^{5/2} \left(\frac{m_\chi + m_Y}{m_\chi + m_X} \right) \, , \tag{44}$$

which hold for the expectation values of these quantities as can be seen from Eqs.(34) and (40). Remarkably, the expectation values of the factors in front of the expressions in square brackets are in fact the same in Eqs.(36) and (42), apart from the factor $1/|n|$ appearing in the former equation. On the other hand, the expressions inside these square parentheses do depend on $f_1(v)$, as well as on the involved masses and form factors.

It is nevertheless instructive to study the behavior of the factor κ for different target nuclei X and Y. This largely determines what choice of targets is optimal, i.e., minimizes the statistical errors of our estimators of m_χ. It is easy to see that the ratio κ/m_χ, which will appear in the relative error $\sigma(m_\chi)/m_\chi$, only depends on the dimensionless ratios m_X/m_χ and m_Y/m_χ. In Fig. 1 we therefore show contours of κ/m_χ in the plane spanned by these two ratios, using the ordering $m_Y > m_X$. We note first of all that κ diverges as $m_Y \to m_X$. This is clear from the fact that the denominator in the final expression in Eq.(43) vanishes in this limit, while the
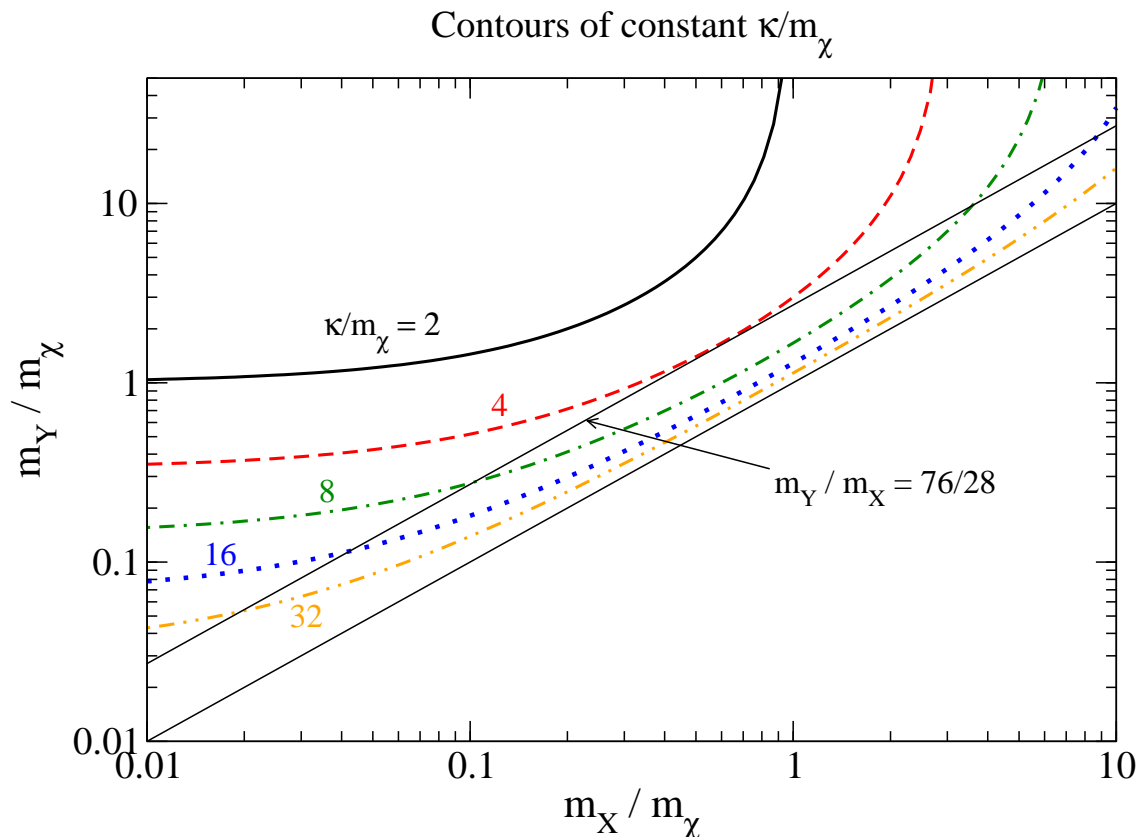
Figure 1: The five thick lines show contours of constant κ/m_χ in the plane spanned by m_X/m_χ and m_Y/m_χ, where we have taken $m_Y > m_X$ without loss of generality. Here κ, has been defined in Eq.(43); recall that the final relative error on m_χ is directly proportional to κ/m_χ. The lower thin line indicates the end of the physical region, $m_Y = m_X$, whereas the upper thin line shows $m_Y = (76/28)m_X$, corresponding to Silicon and Germanium targets.

numerator is finite. Physically this simply means that performing two scattering experiments with the same target will not allow one to determine m_χ.

Slightly less trivially, we also see that κ/m_χ, and hence the relative error on m_χ, becomes very large if both target nuclei are either much heavier or both much lighter than the WIMP. This can be understood from the fact that m_χ only enters via the reduced mass defined in Eq.(3).* If $m_\chi \gg m_N$, $m_{r,N} \to m_N$ becomes completely independent of the WIMP mass. In the opposite extreme, $m_\chi \ll m_N$, $m_{r,N} \to m_\chi$ becomes independent of the mass of the target nucleus, i.e., one is effectively back in the situation where both experiments are performed with the same target.

These considerations favor chosing the two targets to be as different as possible. However, there are limits to this. On the one hand, taking a very light target nucleus will lead to a low event rate for this experiment, and hence very large statistical errors. Since the errors of both experiments are added in quadrature inside the expressions in square parenthesis in Eqs.(36) and (42), this would lead to a large overall error on m_χ. In fact, if the total event number is

---

*Eq.(38) seems to have additional m_χ dependence. However, this comes from the factor $n_\chi = \rho_0/m_\chi$, which drops out when the ratio of two targets is considered.

held fixed, the final error on m_χ will be minimal if both experiments contain approximately the same number of events.

On the other hand, taking a very heavy target nucleus also leads to problems. Heavy nuclei are large, which means they have quite soft form factors. For example, the Woods–Saxon prediction [16] for the form factor for ^{136}Xe, which is the target in some existing experiments [15], has a zero at $Q \simeq 95$ keV. For our default choice $v_{\rm esc} = 700$ km/s, this is below $Q_{\rm max,kin}$ of Eq.(8) for all $m_\chi > 45$ GeV. This is a serious problem, since the form factor, and hence the event rate, remain (very) small even beyond this zero. Experiments with ^{136}Xe therefore effectively impose a cut $Q_{\rm max} \leq 95$ GeV.[†]

From these considerations it seems that chosing $X = {\rm Si}$, $Y = {\rm Ge}$ might be a good compromise. This corresponds to points on the upper, thin solid straight line in Fig. 1. We see that in this case $\kappa/m_\chi \geq 4$ for all values of m_χ. Not surprisingly, κ/m_χ reaches its minimum when m_χ lies in between the masses of the two target nuclei, i.e for the case at hand, for $m_\chi \simeq 50$ GeV. Note also that κ/m_χ is unfortunately always well above unity. One will thus have to get fairly accurate estimates of the relevant integrals I_i if one wishes to determine m_χ to better than a factor of two.

Before discussing the statistical uncertainty in more detail, we proceed to include non–trivial upper and lower cuts on the recoil energy in our analysis.

3.2 Incorporating cuts on the recoil energy

As noted earlier, real experiments will probably have to impose both lower and upper limits on the recoil energy, partly for instrumental reasons, and partly to suppress backgrounds. This led us to introduce generalized moments of f_1 in Eq.(12). These moments determined by two different detectors will still be the same, if either the integration limits are identical, $v_{i,X} = v_{i,Y}$, $i = 1,\ 2$, or the cuts are so loose that the contribution from WIMPs with $v < v_1$ or $v > v_2$ is negligible; a combination of these two possibilities can also occur, e.g., small but not necessarily equal values of $v_{1,X}$ and $v_{1,Y}$, and $v_{2,X} = v_{2,Y}$ significantly below $v_{\rm esc}$.

The crucial observation that forms the basis for our analysis of m_χ as estimated from the generalized moments is that in fact *all three* terms in the final expression in Eq.(12) will agree *separately* between two targets, as long as both integration limits coincide. This can be shown by replacing the $r(Q_i)$ in Eq.(12) via Eq.(1) and using Eq.(15). In principle we could therefore simply equate the last (integral) terms between the two targets. This would lead to expressions very similar to those derived in the previous subsection, the only difference being that all integrals or sums over recoil energies would run over limited ranges.

The problem with this approach is that the velocities v_i appearing in Eq.(12) are not directly observable. The recoil energies are. However, the values of $Q_{\rm min}$ and $Q_{\rm max}$ would need to be *different* for the two targets, if they are to correspond to the same values of v_1 and v_2. Worse, Eq.(15) shows that the ratios $Q_{{\rm min},X}/Q_{{\rm min},Y}$ and $Q_{{\rm max},X}/Q_{{\rm max},Y}$ that one has to chose in order to achieve $v_{i,X} = v_{i,Y}$ depend on m_χ. We are thus faced with the situation that, in the presence of significant cuts on the recoil energy, the quantity we wish to determine is needed as an input at an early stage of the analysis!

This statement is, strictly speaking, true; we see no way around this, if significant cuts on the recoil energy are indeed needed. However, we can alleviate the situation. To begin with, we noticed that the systematic error one introduces by simply setting $Q_{{\rm min},X} = Q_{{\rm min},Y}$ is reduced greatly if one keeps the sum of the first and third terms in Eq.(12). Moreover, we will show

---

[†]Note also that while the integrals I_n remain finite where the form factor vanishes, the estimates for the errors will diverge there, due to the factor $1/F^4$ appearing in Eq.(26).

that, to some extent at least, one can do the matching of two $Q_{\max}$ values for the two targets directly from the data. In principle we could reduce the systematic error associated with the choice of $Q_{\max}$ even more by also including the second term in Eq.(12). However, with limited statistics the error on $r(Q_{\max})$ will always be very large, so that keeping this term will not help significantly.

Our determination of m_χ from generalized moments of f_1 is thus based on equating the sum of the first and third terms in Eq.(12) for two different targets. The resulting expression for m_χ can still be cast in the form of Eq.(34), but $\mathcal{R}_n$ is now given by

$$\mathcal{R}_n(Q_{\min}) = \left[\frac{2Q_{\min,X}^{(n+1)/2} r_X(Q_{\min,X})/F_X^2(Q_{\min,X}) + (n+1)I_{n,X}}{2Q_{\min,X}^{1/2} r_X(Q_{\min,X})/F_X^2(Q_{\min,X}) + I_{0,X}} \right]^{1/n} (X \longrightarrow Y)^{-1} . \qquad (45)$$

Here $n \neq 0$ and $r_{(X,Y)}(Q_{\min,(X,Y)})$ refer to the counting rate for detectors X and Y at the respective lowest recoil energies included in the analysis. They can be estimated from Eq.(24); of course, the values of r_1, k_1, $Q_{s,1}$, and b_1 will in general differ for the two targets. Note that the integrals I_n, I_0 are now to be evaluated with $Q_{\min}$ as lower and $Q_{\max}$ as upper limits, as in Eq.(25).
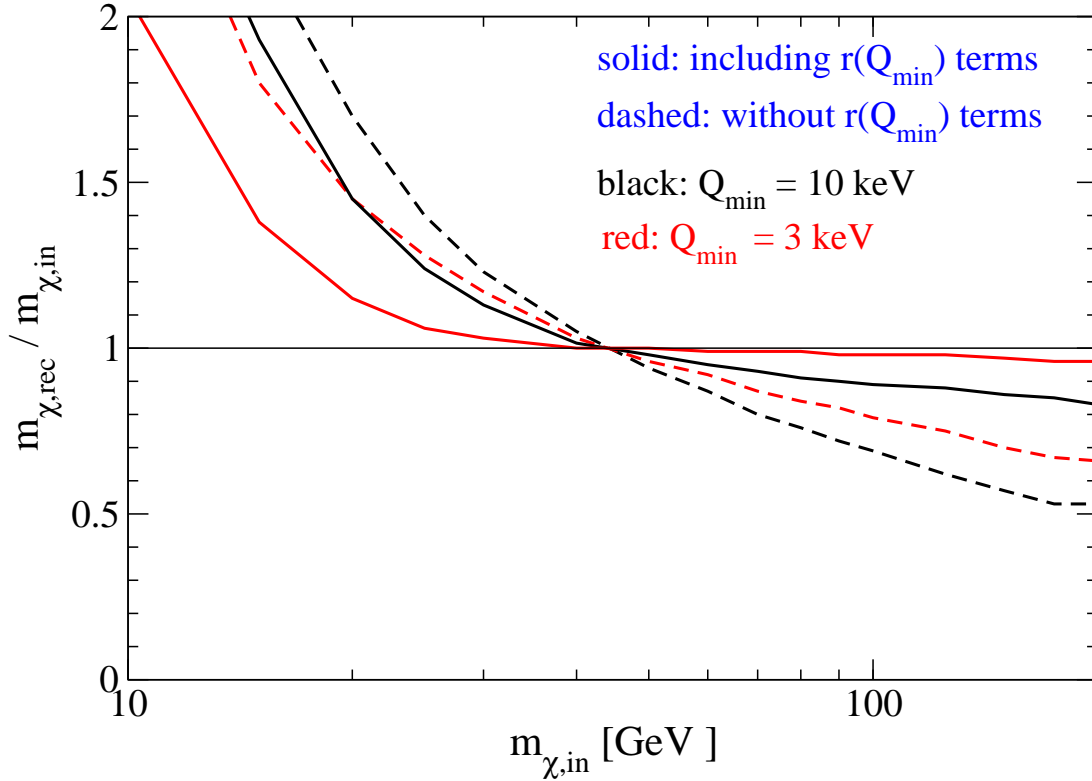

Figure 2: Ratio of reconstructed to input WIMP mass for imperfect $Q_{\min}$ matching, for two different values of $Q_{\min}$. We have taken Si and Ge targets and assumed infinite statistics and (effectively) no upper cut on the recoil energy. The solid (dashed) curves have been computed from Eqs.(34) and (45) with $n = 1$ including (neglecting) all terms $\propto r(Q_{\min})$. See the text for further details.

Before discussing the statistical uncertainty of this estimate of the WIMP mass, we wish to demonstrate that keeping the terms $\propto r(Q_{\min})$ in Eq.(45) indeed reduces the systematic error. This is demonstrated in Fig. 2, which shows the ratio of the reconstructed to input WIMP mass for experiments with "infinite" statistics. Here we have chosen $X = {}^{28}\text{Si}$ and $Y = {}^{76}\text{Ge}$, and we have set $Q_{\max} = \infty$ in order to isolate the systematic effect due to imperfect matching of the $Q_{\min}$ values in this figure.[‡] Here the black (red) curves have been obtained with $Q_{\min,\,\text{Ge}} = Q_{\min,\,\text{Si}} = 10$ (3) keV. The solid lines include the terms $\propto r(Q_{\min})$, while the dashed ones do not. Clearly including these terms is beneficial: for $m_\chi > 20$ GeV, the systematic shift with these terms included and $Q_{\min} = 10$ keV is smaller than that without those terms with the much smaller $Q_{\min} = 3$ keV. We also see that the systematic effect becomes large at small m_χ. This is not surprising, since a small m_χ implies a small $Q_{\max,\text{kin}}$, so that the lower cut on Q removes a correspondingly larger fraction of the total spectrum. The systematic error vanishes for $m_\chi = \sqrt{m_X m_Y} = 43$ GeV, since for this value of m_χ we have $\alpha_X = \alpha_Y$, i.e., $v_{1,X} = v_{1,Y}$ if $Q_{\min,X} = Q_{\min,Y}$. For larger m_χ the systematic effect changes sign, i.e., one now underestimates the true value of m_χ. However, if the terms $\propto r(Q_{\min})$ are included, the shift remains relatively small even for $Q_{\min} = 10$ keV. If values $Q_{\min} \lesssim 3$ keV can be achieved, which should be possible [17], the systematic effect due to imperfect $Q_{\min}$ matching will be a concern only for very light WIMPs, $m_\chi < 20$ GeV.

Using Eq.(45) in Eq.(34) also leads to a lengthier expression for the statistical error on our estimate of m_χ. The first equation in (36) still holds, but the $r(Q_{\min})$ terms give additional contributions to the final expression:

$$
\sigma(m_\chi)|_{\langle v^n \rangle} = \frac{\sqrt{m_X/m_Y}\,|m_X - m_Y|}{\left(\mathcal{R}_n - \sqrt{m_X/m_Y}\right)^2}
$$
$$
\times \left[\sum_{i,j=1}^{3} \left(\frac{\partial \mathcal{R}_n}{\partial c_{i,X}}\right)\left(\frac{\partial \mathcal{R}_n}{\partial c_{j,X}}\right) \text{cov}(c_{i,X} c_{j,X}) + (X \longrightarrow Y) \right]^{1/2}. \tag{46}
$$

Here we have introduced a short–hand notation for the six quantities on which the estimate of m_χ depends:

$$
c_{1,X} = I_{n,X}\,; \qquad c_{2,X} = I_{0,X}\,; \qquad c_{3,X} = r_X(Q_{\min,X})\,, \tag{47}
$$

and similarly for the $c_{i,Y}$. Estimators for $\text{cov}(c_i, c_j)$ have been given in Eqs.(26) and (31). Explicit expressions for the derivatives of $\mathcal{R}_n$ with respect to these six quantities are collected in the Appendix. Note that a factor $\mathcal{R}_n$ can be factored out of all these derivatives. With this factor moved out of the square brackets, the prefactor in Eq.(46) is identical to that in Eq.(36), i.e., its expectation value will again be given by κ of Eq.(43). Of course, Eq.(46) reduces to Eq.(36) in the limit $Q_{\min,X}, Q_{\min,Y} \to 0$. Note finally that Eq.(46) also holds for $n = -1$, if the derivatives with respect to $c_{1,(X,Y)}$ are neglected, since in this case $I_{n,X}$ and $I_{n,Y}$ do not contribute to $\mathcal{R}_n$ given in Eq.(45).

Finite lower energy cuts $Q_{\min,(X,Y)}$ can also easily be incorporated in the quantity $\mathcal{R}_\sigma$ appearing in Eq.(40):

$$
R_\sigma = \frac{\mathcal{E}_Y}{\mathcal{E}_X} \left[\frac{2Q_{\min,X}^{1/2} r_X(Q_{\min,X})/F_X^2(Q_{\min,X}) + I_{0,X}}{2Q_{\min,Y}^{1/2} r_Y(Q_{\min,Y})/F_Y^2(Q_{\min,Y}) + I_{0,Y}} \right]. \tag{48}
$$

[‡]More exactly, for $m_\chi > 100$ GeV we have set $Q_{\max,\,\text{Ge}} = 250$ keV, in order to avoid complications due to the zero of the form factor of ${}^{76}\text{Ge}$ which occurs at $Q \simeq 270$ keV. We have then matched $Q_{\max,\,\text{Si}}$, so that the only systematic deviation of the reconstructed WIMP mass is indeed due to imperfect $Q_{\min}$ matching.

Correspondingly, Eq.(42) changes to

$$\sigma(m_\chi)|_\sigma = \frac{(m_X/m_Y)^{5/2}\,|m_X - m_Y|}{\left[\mathcal{R}_\sigma - (m_X/m_Y)^{5/2}\right]^2}$$

$$\times \left[\sum_{i,j=2}^{3} \left(\frac{\partial \mathcal{R}_\sigma}{\partial c_{i,X}}\right)\left(\frac{\partial \mathcal{R}_\sigma}{\partial c_{j,X}}\right)\text{cov}(c_{i,X}c_{j,X}) + (X \longrightarrow Y)\right]^{1/2}, \qquad (49)$$

where we have again used the short–hand notation of Eq.(47); note that $c_{1(X,Y)}$ does not appear here. Expressions for the derivatives of $\mathcal{R}_\sigma$ are also given in the Appendix.

3.3 Combined fit

In the next step we wish to combine our estimators (34) for different n with each other, and with the estimator (40). This could be done via an overall covariance matrix describing the errors of these estimators and their correlations. The diagonal entries of this covariance matrix are given by Eqs.(46) and (49); the off–diagonal entries can be computed analogously. This would yield the overall best–fit value of m_χ as well as its Gaussian error.

Here we pursue a slightly different procedure, based on a χ^2 fit. This will yield the same best–fit value of m_χ, which we denote by $m_{\chi,\text{rec}}$, but it has two advantages. First, $\chi^2(m_{\chi,\text{rec}})$ can be used as a measure of the quality of the fit, which in turn can be used to match the Q_{max} values of the two experiments at least approximately. Secondly, it allows to determine asymmetric error intervals. Fig. 1 implies that the errors should indeed be asymmetric. For example, if the true m_χ is (much) larger than the masses of both target nuclei, the experimental upper bound one can derive will be quite large or even infinite, but one should still get a meaningful lower bound; the opposite is true if m_χ lies well below the mass of both target nuclei.

We begin by defining fit functions

$$f_{i,X} = \alpha_X^i \left[\frac{2Q_{\min,X}^{(i+1)/2} r_X(Q_{\min,X})/F_X^2(Q_{\min,X}) + (i+1)I_{i,X}}{2Q_{\min,X}^{1/2} r_X(Q_{\min,X})/F_X^2(Q_{\min,X}) + I_{0,X}}\right]\left(\frac{300 \text{ km}}{\text{s}}\right)^{-i}, \qquad (50a)$$

for $i = -1,\ 1,\ 2,\ \ldots,\ n_{\text{max}}$; and

$$f_{n_{\text{max}}+1,X} = \mathcal{E}_X\left[\frac{A_X^2}{2Q_{\min,X}^{1/2} r_X(Q_{\min,X})/F_X^2(Q_{\min,X}) + I_{0,X}}\right]\left(\frac{\sqrt{m_X}}{m_\chi + m_X}\right); \qquad (50b)$$

we analogously define $n_{\text{max}} + 2$ functions $f_{i,Y}$. Here n_{max} determines the highest (generalized) moment of f_1 that is included in the fit. The f_i are normalized such that they are dimensionless and very roughly of order unity; this alleviates numerical problems associated with the inversion of their covariance matrix. The first $n_{\text{max}} + 1$ functions f_i are basically our estimators (23) of the generalized moments defined in Eq.(12) with the term $\propto r(Q_{\text{max}})$ omitted; as discussed earlier, the error on this quantity is likely to be so large that including this term will not be helpful. The last function is essentially the ratio appearing in Eq.(39). It is important to note that m_χ in Eqs.(50a) and (50b) is a fit parameter, not the true (input) value of the WIMP mass. Recall also that our estimator (25) for the integrals I_n appearing in Eqs.(50a) and (50b) is independent of m_χ. Hence the first $n_{\text{max}} + 1$ fit functions depend on m_χ only through the overall factor α^i.

The f_i allow us to introduce a χ^2 function:

$$\chi^2 = \sum_{i,j}\left(f_{i,X} - f_{i,Y}\right)\mathcal{C}_{ij}^{-1}\left(f_{j,X} - f_{j,Y}\right). \qquad (51)$$

Here $\mathcal{C}$ is the total covariance matrix. Since the X and Y quantities are statistically completely independent, $\mathcal{C}$ can be written as a sum of two terms:

$$\mathcal{C}_{ij} = \mathrm{cov}\,(f_{i,X}, f_{j,X}) + \mathrm{cov}\,(f_{i,Y}, f_{j,Y})\,. \tag{52}$$

The entries of this matrix involving only the moments of the WIMP velocity distribution can be read off Eq.(82) of Ref. [14], with an obvious modification due to the normalization factor in Eq.(50a). Since the last f_i can be computed from the same basic quantities, i.e., the counting rates at Q_{min} and the integrals I_0, the entries of the covariance matrix involving this last fit function can also be computed straightforwardly, using Eqs.(26)–(31). Of course, Eq.(51) can also be used to compute asymmetric error intervals from a single moment, by restricting the sum to a single term.

4   Numerical results

We are now ready to present some numerical results for the reconstructed WIMP mass. These results are based on Monte Carlo simulations of direct detection experiments. We assume that the scattering cross section is dominated by spin–independent interactions, and use the Woods–Saxon form for the elastic form factors $F(Q)$ [16]. We describe the WIMP velocity distribution by a sum of a shifted Gaussian contribution [6] and a "late infall" component [12]; as in Ref. [14], for simplicity we model the latter as a $\delta-$function, keeping the normalization $N_{\mathrm{l.i.}}$ of this component as free parameter:

$$f_1(v) = \frac{(1 - N_{\mathrm{l.i.}})}{\sqrt{\pi}}\left(\frac{v}{v_e v_0}\right)\left[\mathrm{e}^{-(v-v_e)^2/v_0^2} - \mathrm{e}^{-(v+v_e)^2/v_0^2}\right] + N_{\mathrm{l.i.}}\delta(v - v_{\mathrm{esc}})\,. \tag{53}$$

We take $v_0 = 220$ km/s, $v_e = 1.05\,v_0{}^{\S}$, and $v_{\mathrm{esc}} = 700$ km/s.

In Fig. 3 we show upper and lower bounds on the reconstructed WIMP mass, calculated from the requirement that χ^2 exceeds its minimum by 1, for the idealized scenario where no cuts on Q have been applied. We took our default set of parameters, i.e., vanishing late infall component, and target nuclei $X = {}^{28}$Si, $Y = {}^{76}$Ge. This figure is based on simulating $2 \times 5{,}000$ experiments, where each experiment contains an expected 50 events; the actual number of events is Poisson–distributed around this expectation value. As mentioned earlier, taking equal numbers of events in both experiments minimizes the statistical error for fixed total number of events. As discussed in Ref. [14], the error on the (high) moments is not quite Gaussian; the deviation becomes larger for smaller samples. The reason is that the high moments receive large contributions from the region of high Q, where on average very few events will lie; even the region where on average only a fraction of an event lies can contribute significantly. As a result, most simulated experiments will underestimate these moments, while a few (rare) experiments will overestimate them. In order to alleviate this problem, we only include moments up to $n_{\mathrm{max}} = 2$ in our fit. Moreover, we always show median, rather than mean, values for the (bounds on the) reconstructed WIMP mass.

We see that the minus–first moment by itself leads to very poor bounds on m_χ. This is not surprising, since its error is dominated by the error on the counting rate at Q_{min}, which is determined only from the events in the first bin. The higher moments lead to increasingly tighter bounds. However, the higher moments are very strongly correlated. Also, the systematic effect due to the limited event samples discussed in the previous paragraph becomes larger for larger n;

---

§Strictly speaking, v_e should oscillate around $1.05\,v_0$ with a period of one year [6]; we ignore this time dependence here.
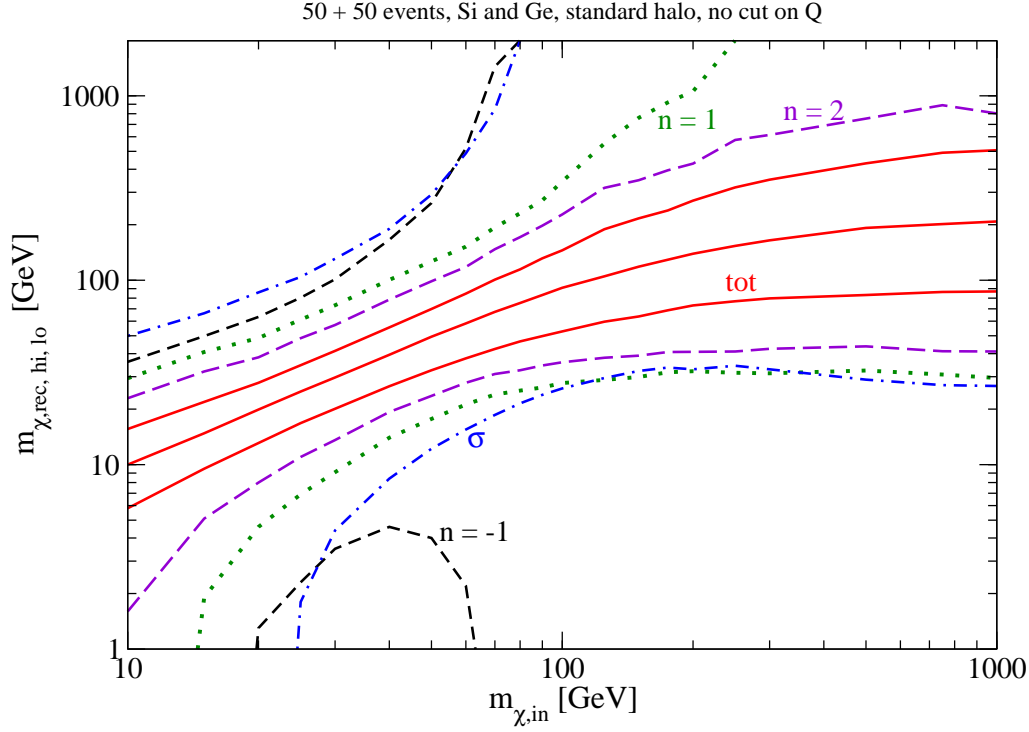
Figure 3: Median values of "$1\,\sigma$" upper and lower bounds on the reconstructed WIMP mass in $2 \times 5{,}000$ simulated experiments with Si and Ge targets, as a function of the true value of m_χ. We generated on average 50 events per experiment. The short–dashed (black), dotted (green) and long–dashed (violet) curves show the upper and lower bounds on m_χ as determined from moments with $n = -1, 1$ and 2, respectively; the dash-dotted (blue) curves labeled σ show the corresponding limits derived from our assumption of equal cross sections for scattering on protons and neutrons. Finally, the solid (red) curves show the upper and lower bound as well as the median reconstructed m_χ for the global fit based on minimizing χ^2 of Eq.(51) with $n_{\max} = 2$. These results are for our standard halo, i.e., no late infall component, without any cuts on the recoil energy.

for example, for $n = 2$ and a true $m_\chi = 1$ TeV, the median upper end of the (nominal) $1\,\sigma$ range lies well below 1 TeV. The lower bound on m_χ derived from the assumption of equal scattering cross sections on protons and neutrons is similar to that derived from the first moment, but the corresponding upper bound is significantly worse. Nevertheless, this estimator of m_χ helps in narrowing down the error of the total fit, described by the upper and lower solid (red) curves. As expected from Fig. 1 the relative error on m_χ is minimal for $m_\chi = \sqrt{m_X m_Y}$, although the increase towards smaller m_χ is less than expected from the behavior of the kinematical factor κ alone.

Unfortunately we also see that the median reconstructed m_χ starts to deviate from the input value if $m_\chi \gtrsim 80$ GeV. This is a direct consequence of the fact that the median value of the estimators of the higher moments is too small, as discussed above. For very large m_χ the median reconstructed WIMP mass even becomes independent of its true value; this is true also for the upper end of the error band. This systematic shift presents another argument in favor of imposing an upper cut $Q_{\max}$ on Q, chosen sufficiently low that an average experiment will still have a few events not too far below $Q_{\max}$.
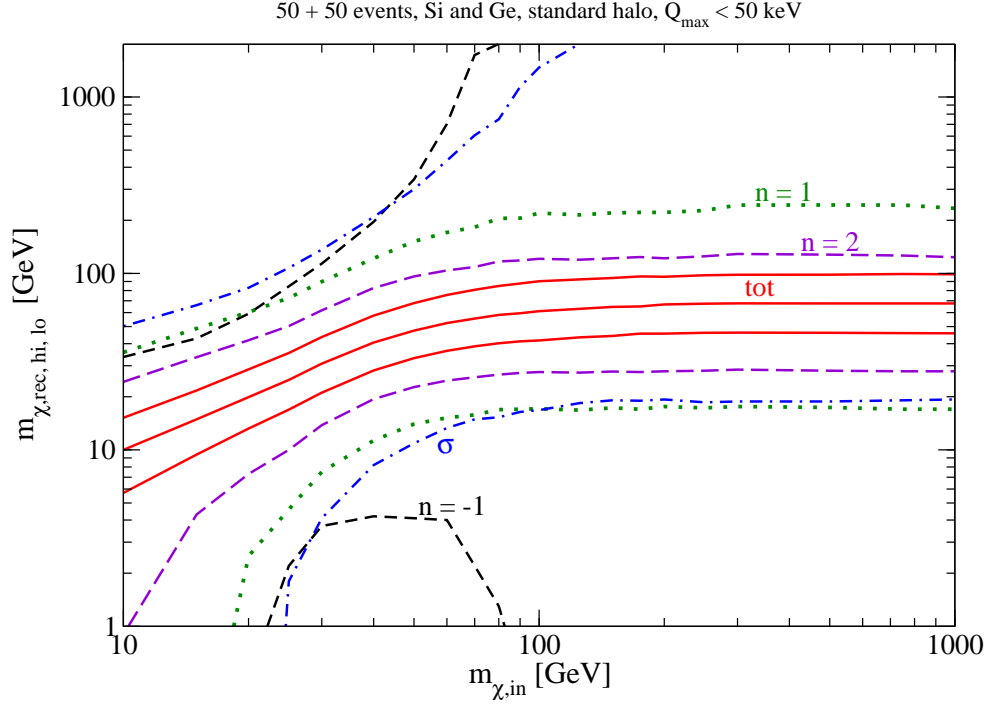
Figure 4: As in Fig. 3, except that we have imposed the cut $Q_{max} = 50$ keV in both experiments. Note that the average of 50 events per experiment refers to the entire Q range, i.e., the number of events after cuts is smaller if $Q_{max,kin} > Q_{max}$.
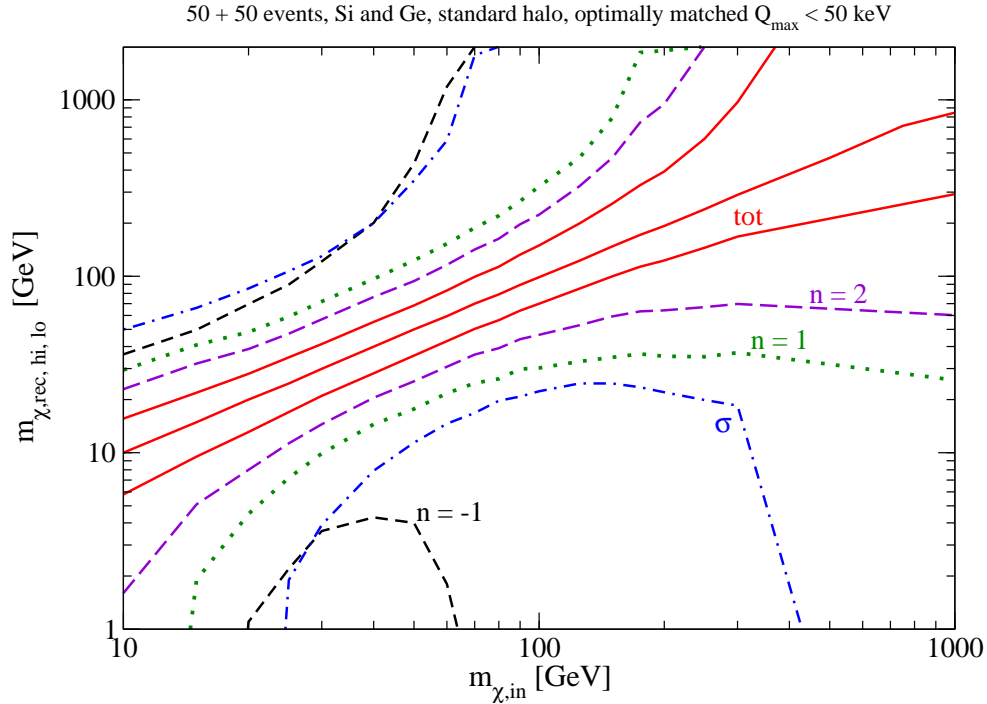

Figure 5: As in Fig. 4, except that we have imposed the cut $Q_{max} = 50$ keV for the Ge target. The value of Q_{max} for the Si target has been chosen such that it corresponds to the same WIMP velocity.

For the case at hand, with rather small event samples, this would imply $Q_{\max} \simeq 50$ keV. Unfortunately Fig. 4 shows that simply imposing the same cut on $Q_{\max}$ in both targets makes the situation significantly *worse*. Now the median reconstructed m_χ starts to undershoot the input value already at $m_\chi \simeq 60$ GeV, and the asymptotic reconstructed m_χ for large input WIMP mass lies well below 100 GeV. Clearly we need to choose different $Q_{\max}$ values for the two experiments if we want to get reliable results also for larger WIMP masses.

Fig. 5 indicates that this should be possible, at least in principle. Here we have again applied a fixed upper cut $Q_{\max} = 50$ keV for the Ge experiment, but matched the cut on $Q_{\max}$ for the Si experiment such that it corresponds to the same WIMP velocity:

$$Q_{\max,\,\mathrm{Si}} = \left(\frac{\alpha_{\mathrm{Ge}}}{\alpha_{\mathrm{Si}}}\right)^2 Q_{\max,\,\mathrm{Ge}}\,, \tag{54}$$

where α has been given in Eq.(5). We see that now the median reconstructed m_χ indeed tracks the input value even for very large WIMP masses. It should be noted that these results still only use 50 events on average per experiment *before cuts*. For example, for $m_\chi = 500$ GeV Eq.(54) with $Q_{\max,\,\mathrm{Ge}} = 50$ keV implies $Q_{\max,\,\mathrm{Si}} = 21.7$ keV, meaning that the expected number of events in the Si experiments is only about 21. This explains why the error bands at large values of m_χ are significantly wider here than in Fig. 3 where no cuts on the recoil energy have been imposed. Of course, the systematic deviation of the reconstructed m_χ from its true value makes the error bands in Fig. 3 largely meaningless for $m_\chi \gtrsim 100$ GeV.

While the results in Fig. 5 look quite impressive, they suffer from the fact that optimal $Q_{\max}$ matching, as in Eq.(54), is only possible if m_χ is already known. The left frame of Fig. 6 shows
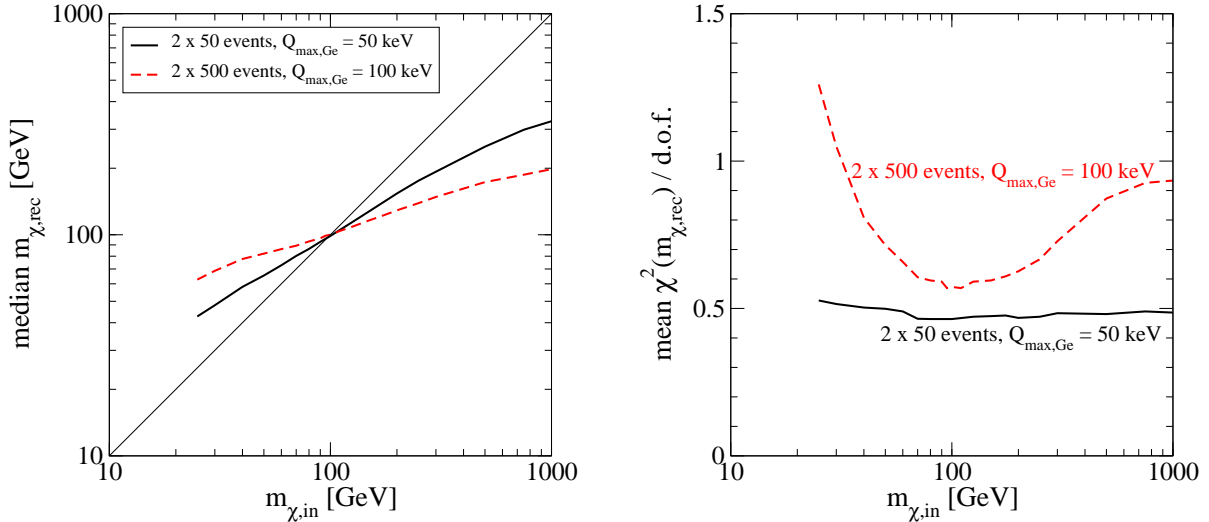

Figure 6: Sensitivity of the χ^2 fit to the value of m_χ that is used as input in the $Q_{\max}$ matching condition (54), assuming a true WIMP mass of 100 GeV, for our default choice of targets and $f_1(v)$. The solid (black) lines are for 2×50 events and $Q_{\max} = 50$ keV, while the dashed (red) curves assume 2×500 events and $Q_{\max} = 100$ keV; here $Q_{\max}$ stands for the bigger of the values used for the two targets, the second one being fixed by Eq.(54). The curves terminate at $m_{\chi,\mathrm{in}} = 25$ GeV since for even smaller WIMP masses, $Q_{\max,\mathrm{kin}} < 50$ keV, making matching superfluous. The left frame shows the median reconstructed WIMP mass from a χ^2 fit with $n_{\max} = 2$, and the right frame shows the corresponding mean value of $\chi^2(m_{\chi,\mathrm{rec}})$.

that inputting the wrong value of m_χ into Eq.(54) will usually lead to a reconstructed WIMP mass in between this input value and the true value. Note that the median $m_{\chi,\mathrm{rec}}$ as a function of $m_{\chi,\mathrm{in}}$ has a slope less than unity. This means that an iteration, where one starts with some input value of m_χ and uses the corresponding $m_{\chi,\mathrm{rec}}$ as new input value into Eq.(54), will converge "on average". Unfortunately our Monte Carlo simulations show that for any one experiment, this procedure does not necessarily converge to a well–defined $m_{\chi,\mathrm{rec}}$; rather, one often ends up in an endless loop over several values of $m_{\chi,\mathrm{rec}}$.

An alternative is to try an algorithm for Q_{max} matching which is based on the minimum value of χ^2 obtained in the fit; recall that this minimum defines the reconstructed WIMP mass. Unfortunately the right frame in Fig. 6 indicates that this may be difficult, at least with the initial small statistics expected. This figure shows that the mean value of $\chi^2(m_{\chi,\mathrm{rec}})$ is almost independent of the value of m_χ input into Eq.(54) if one has only 2×50 events in the sample. The situation looks considerably more promising with 2×500 events, and larger allowed Q_{max}: in this case $\chi^2(m_{\chi,\mathrm{rec}})$ has a clear, if rather broad, minimum where $m_{\chi,\mathrm{in}}$ equals the true WIMP mass, taken to be 100 GeV in this example.

Note that this minimum has mean $\chi^2(m_{\chi,\mathrm{rec}})/\mathrm{d.o.f.}$ well below unity; the same is true for the entire solid curve. Here the number of degrees of freedom is three, since we fit four quantities with one free parameter. This indicates that our numerical procedure on average over–estimates the true errors somewhat. In fact, following Ref. [14], we add the "error on the error" to
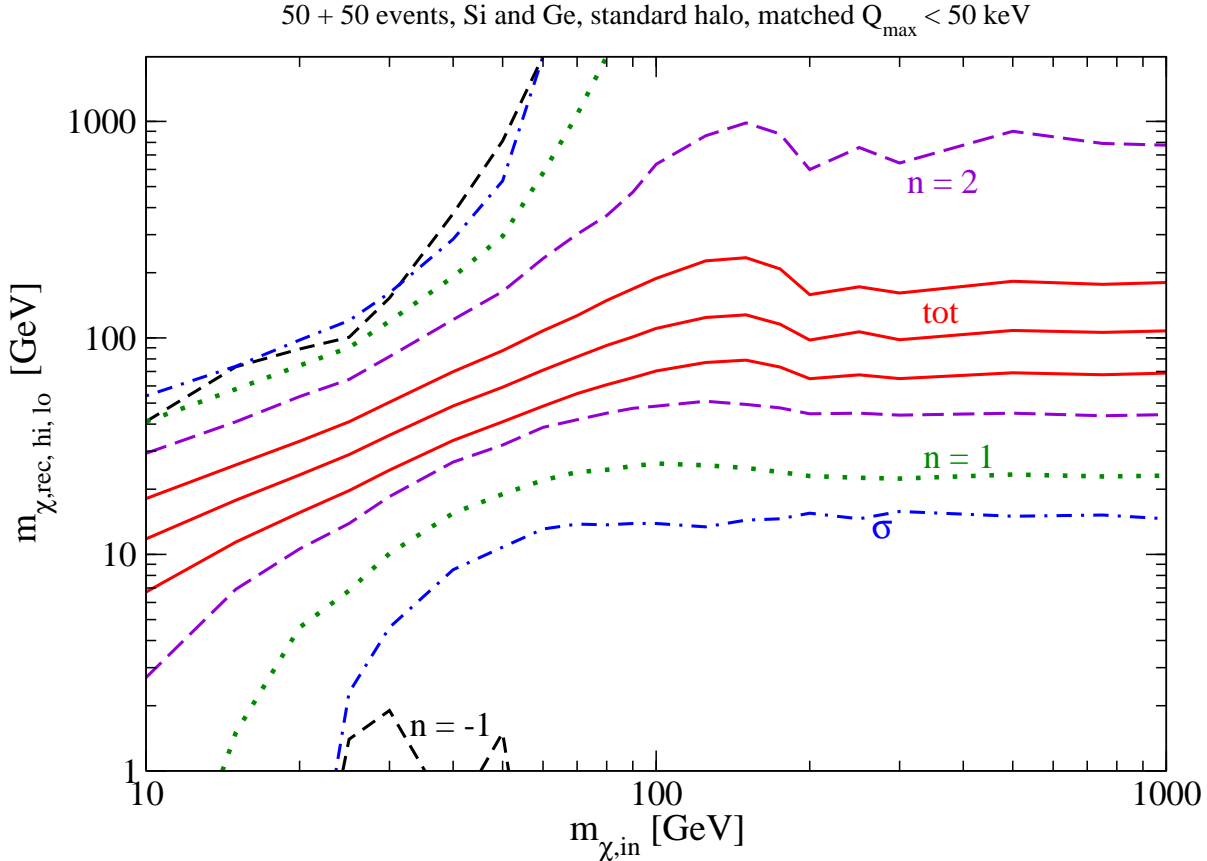

Figure 7: As in Fig. 4, except that we have imposed the fixed cut $Q_{\mathrm{max}} = 50$ keV only on the Ge experiment and determined $Q_{\mathrm{max,Si}}$ by minimizing $\chi^2(m_{\chi,\mathrm{rec}})$.

the diagonal entries of $\mathrm{cov}(I_n, I_m)$, in order to tame non–Gaussian tails in the distribution of measured moments of f_1.

One possibility is to choose the Q_{max} values such that $\chi^2(m_{\chi,\mathrm{rec}})$ is minimal. Note that this implies a double minimization: for fixed values of $Q_{\mathrm{max},X}$ and $Q_{\mathrm{max},Y}$, $m_{\chi,\mathrm{rec}}$ is the WIMP mass that minimizes $\chi^2(m_\chi)$. In an outer loop, Q_{max} is varied. We found that varying both Q_{max} values leads to quite misleading results, especially for larger (true) WIMP masses and/or limited statistics. On the other hand, Fig. 4 shows that for small m_χ, Q_{max} matching is not really necessary; if $m_\chi > \sqrt{m_X m_Y}$, the matching condition (54) implies that Q_{max} for the lighter target should be smaller than that for the heavier target.

In Fig. 7 we have therefore minimized $\chi^2(m_{\chi,\mathrm{rec}})$ *only* for the lighter target, here Silicon. Note that we always require $Q_{\mathrm{max},\mathrm{Si}} \leq Q_{\mathrm{max},\mathrm{Ge}}$ in this procedure; in Fig. 7 the latter is fixed to 50 keV. We see that this leads to a systematic over–estimation of m_χ for small WIMP masses. For heavier WIMPs the results are somewhat better than for the case where both Q_{max} values are simply taken to be equal, see Fig. 4. However, this algorithm clearly still fails quite badly
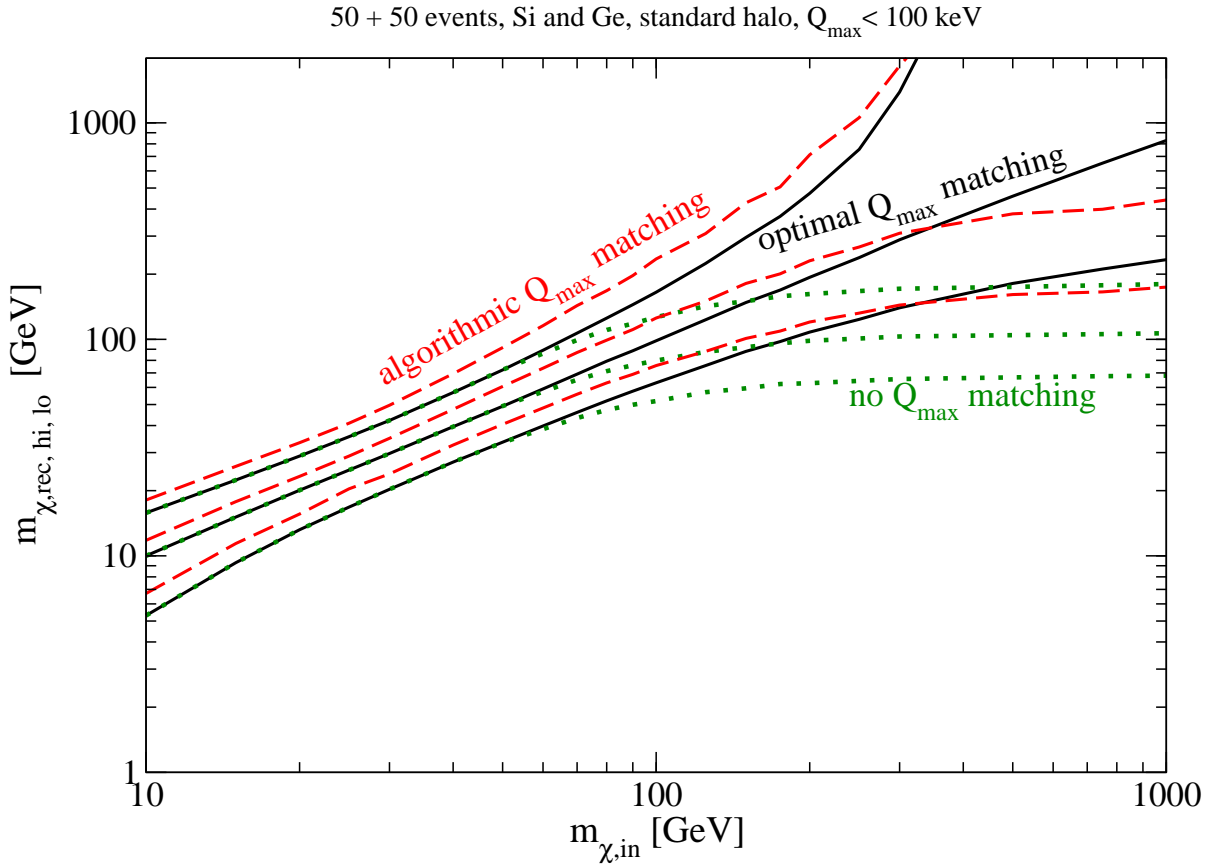

Figure 8: Results for the median value of the reconstructed WIMP mass as well as the ends of its error interval. All results are based on the combined fit, using Eq.(51) with $n_{\mathrm{max}} = 2$. We assume Si and Ge targets with on average 50 events each before cuts, and took our default ansatz for f_1. The dotted (green) lines show results for $Q_{\mathrm{max},\mathrm{Si}} = Q_{\mathrm{max},\mathrm{Ge}} = 100$ keV, whereas the solid (black) lines have been obtained using Eq.(54) with the bigger of the two Q_{max} values fixed to 100 keV. Finally, the dashed (red) lines are for the case that $Q_{\mathrm{max},\mathrm{Ge}} = 100$ keV, whereas $Q_{\mathrm{max},\mathrm{Si}}$ has been chosen such that $\chi^2(m_{\chi,\mathrm{rec}})$ is minimal.

for $m_\chi \gtrsim 100$ GeV. This is partly due to the low maximal value of Q_{max} assumed here. The fact that the kinematic upper bound $Q_{max,kin}$ of Eq.(8) increases with m_χ indicates that the region of large Q is more sensitive to the value of m_χ if the WIMP mass exceeds the mass of the heaviest target nucleus.

In Fig. 8 we have therefore increased the cut Q_{max} to 100 keV; of course, this cut only becomes effective once $Q_{max,kin} > 100$ keV. Unlike in the previous figures, we here show results only for the final fit; the values of m_χ derived from single observables are no longer shown. This allows us to show results for three different choices of $Q_{max,Si}$ and $Q_{max,Ge}$. The dotted (green) curves show the median reconstructed WIMP mass and its "1σ" upper and lower bounds for the case where both Q_{max} values have been fixed to 100 keV. Due to the higher Q_{max} chosen here, this works for considerably larger WIMP masses than in the corresponding Fig. 4, where both Q_{max} values had been fixed to 50 keV. However, for large m_χ the median reconstructed WIMP mass is still only slightly above 100 GeV. The solid (black) lines show results for the case that perfect Q_{max} matching has been applied, using Eq.(54). Comparison with Fig. 5 shows that increasing Q_{max} actually slightly increases the width of the errors on the reconstructed WIMP mass. The reason is that Q_{max} is now so large that the median values of the estimators for the (generalized) moments of f_1 fall somewhat below the true values. Nevertheless the results for this optimal Q_{max} matching remain very encouraging.

Most importantly, our simple algorithm of fixing $Q_{max,Ge}$, in this case to 100 keV, and determining $Q_{max,Si}$ by minimizing $\chi^2(m_{\chi,rec})$ now also seems to work reasonably well for WIMP masses up to ~ 500 GeV. For $m_\chi \lesssim 100$ GeV the median WIMP mass determined in this way again over–estimates its true value by 15 to 20%; however, the median value of the "1σ" lower bound lies below the true WIMP mass for all values of m_χ. Similarly, the median "1σ" upper bound now lies well above the true WIMP mass even for $m_\chi = 1$ TeV, in sharp contrast to the results shown in Fig 7.

We had argued earlier, based on the results of Fig. 1, that Si and Ge is likely to be close to the optimal choice among the target nuclei currently being employed. In Fig. 9 we back this up by showing results analogous to those of Fig. 8, but with Argon and Xenon targets. Since the elastic form factor of ^{136}Xe has a zero near 95 keV, we have lowered the upper bound on Q_{max} to 75 keV; larger values would start to probe the very sparsely populated region near the zero, leading to too small median values of the estimated moments, whereas smaller values would lead to even worse sensitivity to large WIMP masses. We see that, except for small WIMP masses, the results are clearly worse than those shown in Fig. 8.

The starting point of our discussion was that we wanted to devise ways to estimate the WIMP mass which are independent of any assumptions on the WIMP velocity distribution f_1. In order to test this, we have simulated Si and Ge experiments, allowing 25% of the local WIMP flux to come from a "late infall" component, i.e., we fixed $N_{l.i.} = 0.25$ in Eq.(53). The results are shown in Fig. 10. We see that the results are very similar to those with $N_{l.i.} = 0$ shown in Fig. 8 if optimal Q_{max} matching (54) is used. On the other hand, the results for non–optimal choices of Q_{max} get somewhat worse. This is true both for the simple choice $Q_{max,Si} = Q_{max,Ge}$, where significant deviations set in for lower values of the WIMP mass, and for our algorithm of determining $Q_{max,Si}$ by minimizing $\chi^2(m_{\chi,rec})$. In the latter case, the systematic difference between median reconstructed and true WIMP mass is larger than for $N_{l.i.} = 0$, both for small and for large m_χ. The reason for this degradation is that introducing a large late–infall component, corresponding to WIMPs with velocity about three times larger than the mean velocity of the shifted Gaussian component, increases the number of events at large recoil energy. Hence correct Q_{max} matching becomes more important. Note, however, that the true m_χ always lies within the median limits of the "1σ" error interval estimated from our algorithmic Q_{max} matching.
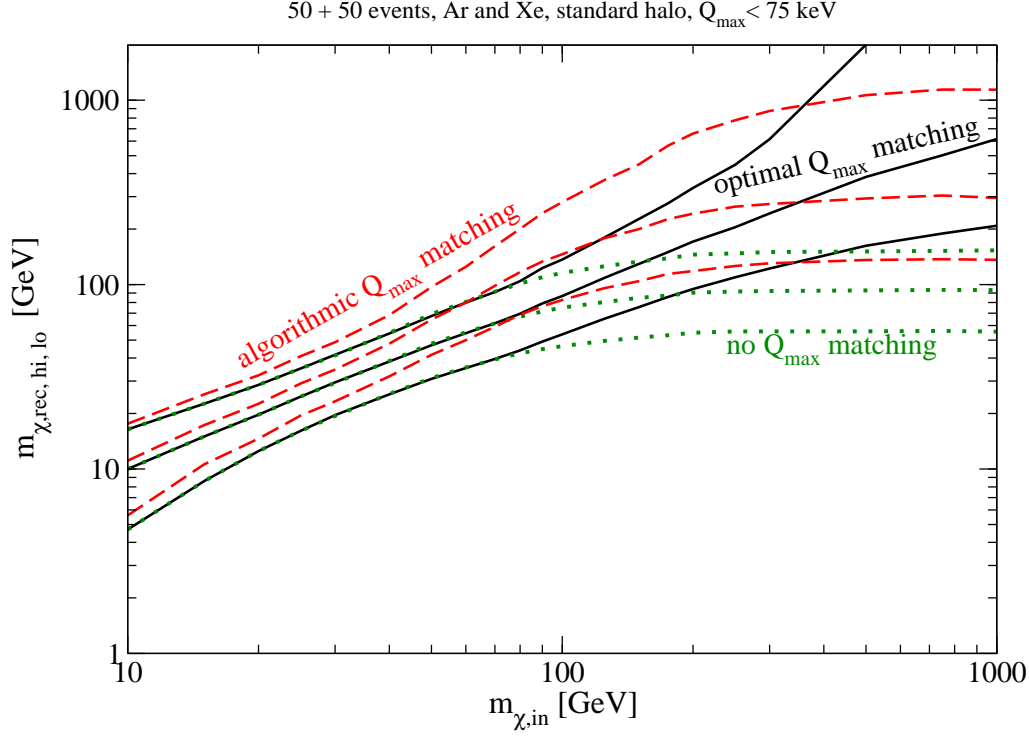
Figure 9: As in Fig. 8, except for ^{40}Ar and ^{136}Xe targets, and with both Q_{max} values restricted to not exceed 75 keV.
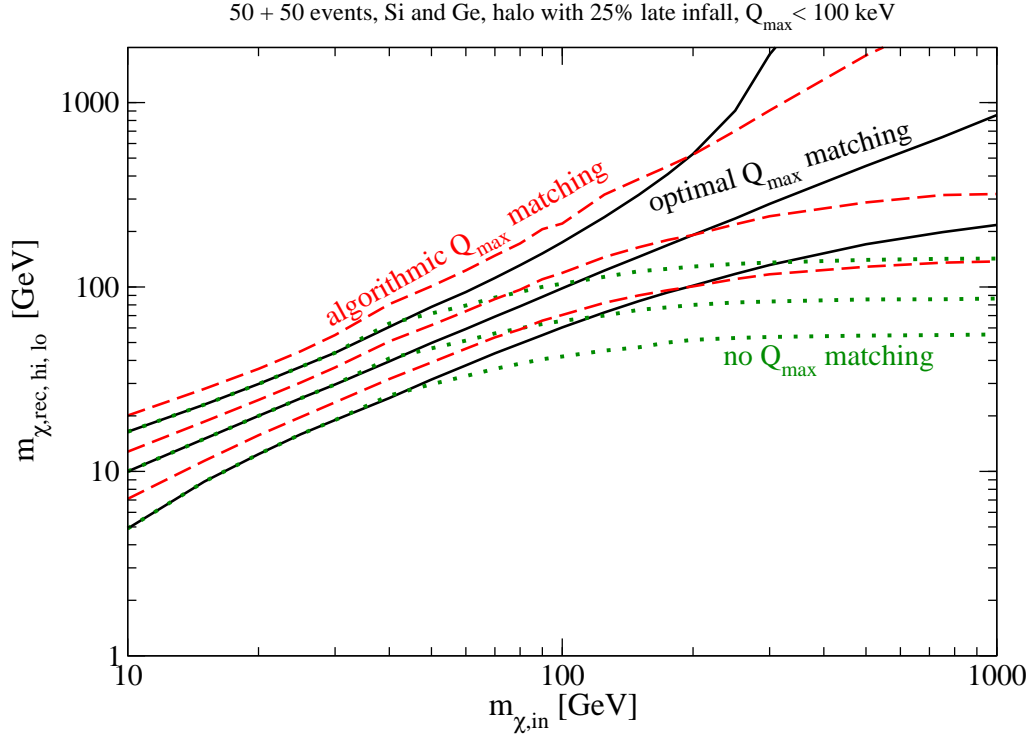

Figure 10: As in Fig. 8, except that we allowed a 25% late infall component in the local WIMP flux, by setting $N_{l.i.} = 0.25$ in Eq.(53).
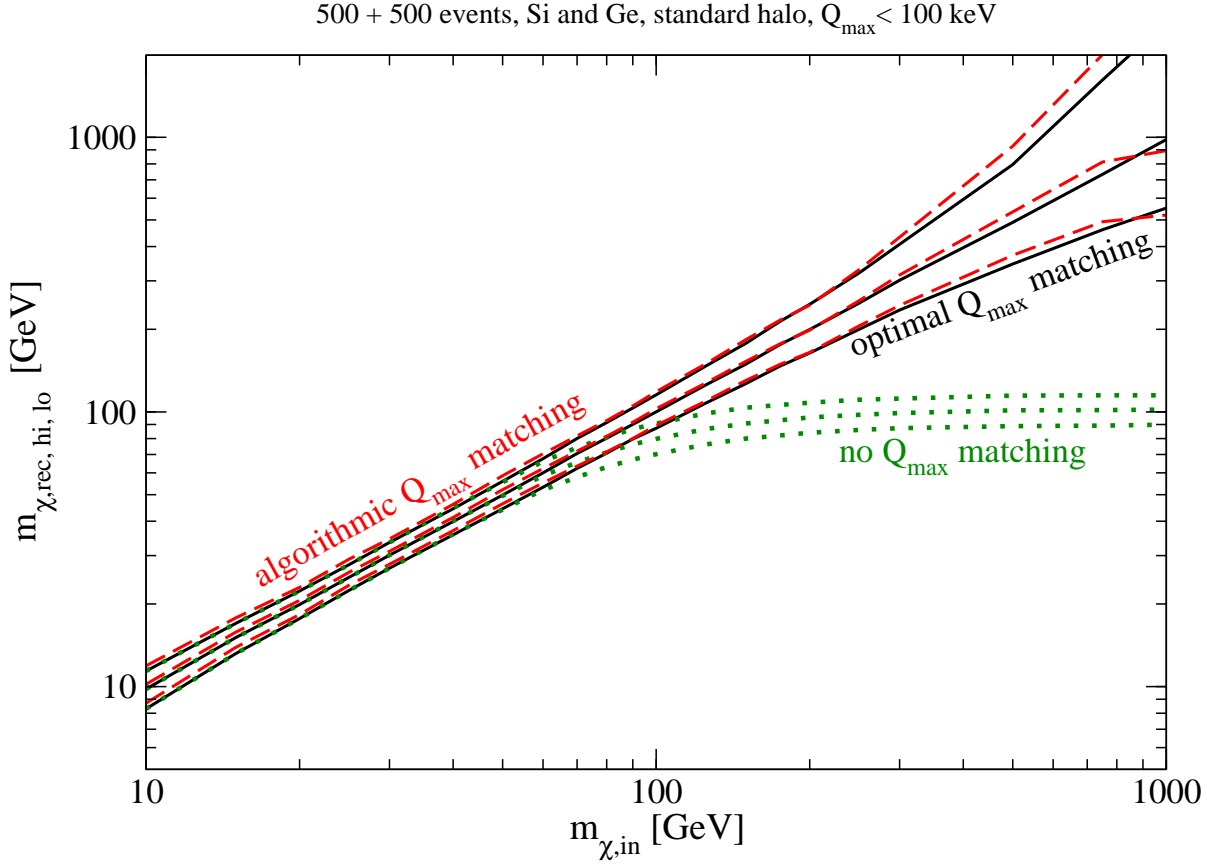
Figure 11: As in Fig. 8, except for 2×500 events before cuts.

So far we have assumed that each experiment "only" has an exposure corresponding to 50 events before cuts. In Fig. 11 we raise this number by a factor of 10. Not surprisingly, all error bars shrink by a factor $\gtrsim 3$ compared to the situation of Fig. 8. The error interval also remains approximately symmetric out to much larger values of m_χ. However, the larger number of events does not significantly change the median reconstructed m_χ if one simply fixes both Q_{max} values to 100 keV. This is not surprising: for large m_χ this implies that $v_{2,Si}$ and $v_{2,Ge}$ in the definition (12) of the generalized moments, and hence the moments themselves, are quite different. Hence the estimators of these moments will not agree if the true WIMP mass is used. On the other hand, our algorithm for fixing $Q_{max,Ge}$ now seems to perform very well over the entire range of WIMP masses shown. In particular, the median reconstructed WIMP mass now overshoots its true value by only a few percent for $m_\chi \lesssim 100$ GeV, and remains close to the true value even at $m_\chi = 1$ TeV. Unfortunately we will see shortly that for large WIMP masses our algorithm still has some problems even in this case.

The problem lies in the distribution of the reconstructed WIMP masses in the simulated experiments. This distribution is supposed to be characterized by the error intervals shown in

Figs. 3–5 and 7–11. In order to see how well this works, we introduce the quantity

$$
\delta m = \begin{cases}
1 + \dfrac{m_{\chi,\mathrm{lo1}} - m_\chi}{m_{\chi,\mathrm{lo1}} - m_{\chi,\mathrm{lo2}}}, & \text{if } m_\chi \leq m_{\chi,\mathrm{lo1}}\,; \\[2ex]
\dfrac{m_{\chi,\mathrm{rec}} - m_\chi}{m_{\chi,\mathrm{rec}} - m_{\chi,\mathrm{lo1}}}, & \text{if } m_{\chi,\mathrm{lo1}} < m_\chi < m_{\chi,\mathrm{rec}}\,; \\[2ex]
\dfrac{m_{\chi,\mathrm{rec}} - m_\chi}{m_{\chi,\mathrm{hi1}} - m_{\chi,\mathrm{rec}}}, & \text{if } m_{\chi,\mathrm{rec}} < m_\chi < m_{\chi,\mathrm{hi1}}\,; \\[2ex]
\dfrac{m_{\chi,\mathrm{hi1}} - m_\chi}{m_{\chi,\mathrm{hi2}} - m_{\chi,\mathrm{hi1}}} - 1, & \text{if } m_\chi \geq m_{\chi,\mathrm{hi1}}\,.
\end{cases}
\tag{55}
$$

Here m_χ is the true WIMP mass, $m_{\chi,\mathrm{rec}}$ its reconstructed value, $m_{\chi,\mathrm{lo1(2)}}$ is the "1 (2) σ" lower bound satisfying $\chi^2(m_{\chi,\mathrm{lo(1,2)}}) = \chi^2(m_{\chi,\mathrm{rec}}) + 1\ (4)$, and $m_{\chi,\mathrm{hi1(2)}}$ are the corresponding "1 (2) σ" upper bounds. In the limit of purely Gaussian errors, where χ^2 of Eq.(51) is simply a parabola, $(\delta m)^2$ would itself be a χ^2 variable, measuring the difference between the true and the reconstructed WIMP mass in units of the error of the reconstruction. However, we saw earlier that
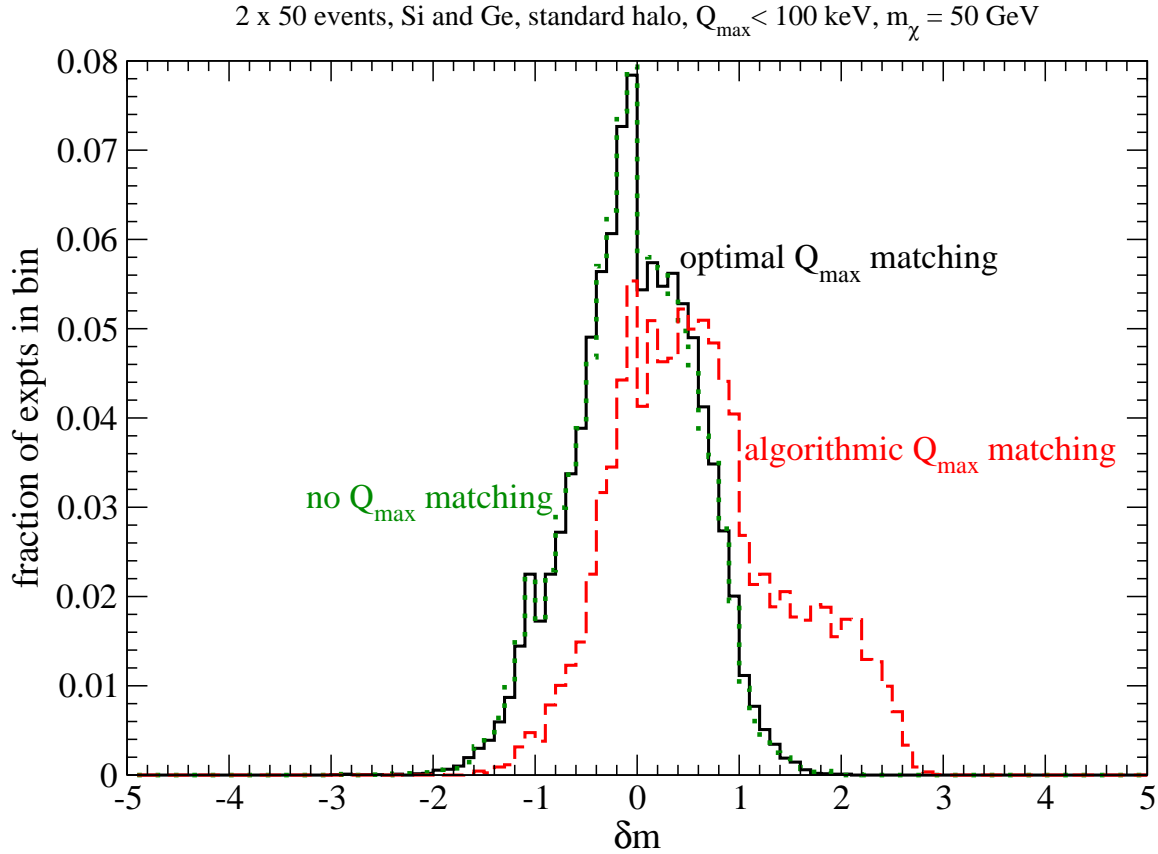

Figure 12: Normalized distribution of the variable δm defined in Eq.(55) for 5,000 simulated experiments, for true WIMP mass $m_\chi = 50$ GeV. The other parameters, are as in Fig. 8. The solid (black) histogram shows results for perfect Q_{max} matching with $Q_{\mathrm{max}} \leq 100$ keV, based on Eq.(54), whereas the dotted (green) histogram is for fixed equal Q_{max} values of 100 keV. The dashed (red) histogram shows results when $Q_{\mathrm{max,Si}}$ is determined by minimizing $\chi^2(m_{\chi,\mathrm{rec}})$.

the error intervals are often quite asymmetric. Similarly, the distance between the "2σ" and "1σ" limits can be quite different from the distance between the "1σ" limit and the central value. The definition (55) takes these differences into account, and also keeps track of the sign of the deviation: if the reconstructed WIMP mass is larger (smaller) than the true one, δm is positive (negative). Moreover, $|\delta m| \leq 1$ (2) if and only if the true WIMP mass lies between the "experimental" 1 (2) σ limits.

In Fig. 12 we show the distribution of δm calculated from 5,000 simulated experiments, assuming a rather small WIMP mass, $m_\chi = 50$ GeV. The other parameters have been fixed as in Fig. 8. In this case simply fixing both Q_{max} values to 100 keV still works fine, since the kinematic maximum values of Q lie only slightly above 100 keV (at 122 keV for Si and 132 keV for Ge). The distributions for fixed Q_{max}, or for optimal Q_{max} matching, look somewhat lopsided, since the error interval is already asymmetric, with $m_{\chi,hi1} - m_{\chi,rec} > m_{\chi,rec} - m_{\chi,lo1}$. As a result, negative values of δm have a larger denominator than positive values, hence the distribution is narrower for $\delta m < 0$. These distributions also indicate that our errors are indeed over–estimated, since nearly 90% of the simulated experiments have $|\delta m| \leq 1$; we remind the reader that a usual 1σ interval should only contain some 68% of the experiments.

We saw in Fig. 8 that our algorithm for determining $Q_{max,Si}$ tends to overestimate the WIMP mass if the latter is small. This is reflected by the dashed (red) histogram in Fig. 12, which has significantly more entries at positive values than at negative values. Moreover, this histogram is rather flat between $\delta m = 1$ and 2. Since our algorithm is based on a double minimization of χ^2 defined in Eq.(51), it is not very surprising that the resulting final $\chi^2(m_{\chi,rec})$ values are distributed quite differently from what one finds after a single minimization step. Nevertheless it is reassuring that some 70% of the simulated experiments lead to $|\delta m| \leq 1$.
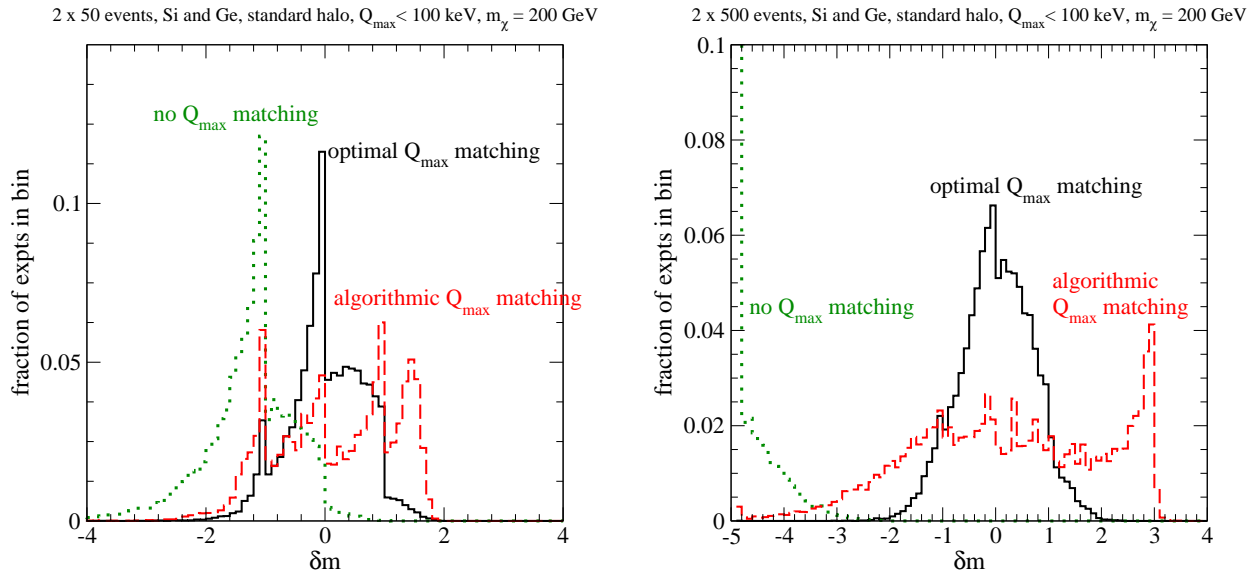

Figure 13: Distribution of δm defined in Eq.(55) calculated from 5,000 simulated experiments. Parameters and notations are as in Fig. 12, except that we have increased the WIMP mass to 200 GeV. In the right frame we have in addition increased the average number of events (before cuts) in each experiment from 50 to 500. Note that the bins at $\delta m = \pm 5$ are overflow bins, i.e., they also contain all experiments with $|\delta m| > 5$.

Unfortunately Fig. 13 shows that the situation becomes much less favorable at the larger WIMP mass of 200 GeV. Here we show results with 50 (left) and 500 (right) events per experiment (before cuts), with the other parameters as in Fig. 12. We see that for optimal $Q_{\max}$ matching a large majority of the simulated experiments still satisfy $|\delta m| \leq 1$. The fact that this fraction decreases from nearly 90% for the smaller events samples to about 85% for the larger samples indicates that our error estimates become a bit more reliable for larger event numbers.[¶] Note also that the secondary peak at $\delta m \simeq -1$ is due to the change of denominator in the definition (55).

We already saw in Figs. 8 and 11 that setting $Q_{\max,\mathrm{Si}} = Q_{\max,\mathrm{Ge}} = 100$ keV significantly under–estimates the true WIMP mass if the latter exceeds 100 GeV. This is borne out by Figs. 13. Since the statistical error decreases with increasing number of events, δm is much smaller in the right frame; in fact, most of the simulated experiments now fall in the "underflow bin" $\delta m = -5$, which also contains all experiments giving even smaller values. In other words, most of the simulated experiments would give a reconstructed WIMP mass more than five estimated standard deviations below the true value, if no $Q_{\max}$ matching is used.

Unfortunately the error estimates resulting from our algorithm of determining $Q_{\max,\mathrm{Si}}$ by minimizing $\chi^2(m_{\chi,\mathrm{rec}})$ are also not very reliable in this case. For the smaller event sample, we find that about 58% of the simulated experiments yield $|\delta m| \leq 1$, while nearly all experiments give $|\delta m| \leq 2$. While these numbers are not so different from the corresponding Gaussian predictions, the distribution of δm is clearly highly non–Gaussian in this case. Just as in the scenario without $Q_{\max}$ matching the error estimates actually become less reliable with increasing event samples. If both experiments contain on average 500 events each, less than 40% of the experiments have $|\delta m| \leq 1$, while more than 30% of the simulations yield $|\delta m| \geq 2$. In fact, the most likely value of δm is now close to 3. In view of these observations, the fact that the median δm is close to zero, so that the median reconstructed WIMP mass is close to the true value as already shown in Fig. 11, seems almost accidental. Recall also that the nominal "1σ" uncertainty of the reconstructed WIMP mass still amounts to about 40 GeV in this case. This means that the most likely value of $m_{\chi,\mathrm{rec}}$ predicted by our algorithm exceeds the true value by more than 100 GeV. This clearly leaves some room for improvements. The fact that optimal $Q_{\max}$ matching continues to give good results for both the reconstructed WIMP mass and its error indicates that better data–based algorithms might very well exist.

5   Summary and Conclusions

In this paper we described methods to determine the mass of a Weakly Interacting Massive Particle detected "directly", i.e., through the recoil energy deposited in a detector by the recoiling nucleus after a WIMP scattered elastically off this nucleus. Our methods are model–independent in the sense that they do not need any assumption about the WIMP velocity distribution. The price one has to pay for this is that one will need positive signals in at least two different detectors, employing different target nuclei.

Our methods are based on our earlier work [14] on reconstructing the WIMP velocity distribution, which we briefly reviewed in Sec. 2. In this earlier work, which was based on results from a single (simulated) experiment, the WIMP mass m_χ was an input. In Sec. 3 we showed how one can determine m_χ by equating results obtained by different experiments. Here the moments of the velocity distribution function are particularly useful, since all events in the sam-

---

[¶]Assuming, unrealistically, that there are 50,000 events in each experiment, we find that only about 75% of all experiments have $|\delta m| \leq 1$, indicating a very slow approach to the Gaussian value of about 68%.

ple contribute to any given moment, leading to relatively low statistical uncertainties. We also described a method for determining m_χ that can be used if the ratio of WIMP scattering cross sections on protons and neutrons is known; this is true, for example, for the spin–independent scattering of supersymmetric neutralinos, where these two cross sections are nearly equal. We also showed how to combine these methods using a χ^2 fitting procedure.

Sec. 4 was devoted to a detailed numerical analysis of our methods. We saw that, assuming the sizes of the event samples are fixed, the statistical errors will be smaller for larger mass difference between the two target nuclei. In practice experiments with heavier targets will accumulate more events, assuming equal exposure, at least if the spin–independent contribution to the scattering cross section dominates. However, the number of useful events (after cuts, preferably in an almost background–free energy range) also depends on other factors, besides the masses of the target nuclei.

In our discussion we saw that, for WIMP masses exceeding 100 GeV or so, the maximal recoil energy $Q_{\max}$ of accepted signal events plays a crucial role. Existing experiments have $Q_{\max} \leq 100$ keV. If both targets used fixed $Q_{\max}$ values of this order or even smaller, a significant systematic error on the extracted WIMP mass results. In principle this problem can be solved by matching the $Q_{\max}$ values of the two experiments. The problem is that perfect matching requires prior knowledge of the WIMP mass. We tried two algorithms to overcome this problem. Determining $Q_{\max}$ of one experiment iteratively should converge "on average", but in a given experiment often leads to an endless loop, rather than a specific value of $Q_{\max}$; this problem is particularly severe for small event samples. On the other hand, determining $Q_{\max}$ of the experiment with the lighter target nucleus by minimizing χ^2 also with respect to this quantity over–estimates the WIMP mass if it is small, and leads to unreliable error estimates if the WIMP mass is larger, the problem becoming worse with increasing event samples. However, the fact that optimal $Q_{\max}$ matching works well in all cases, for both the median reconstructed WIMP mass and its error (which tends to be over–estimated by our expressions), gives us hope that a better algorithm for $Q_{\max}$ matching can be found which only relies on the data. One possibility that might be worth exploring is to employ a combination of an iterative procedure and a second χ^2 minimization, where the latter is used only if the former does not converge to a well–defined value of the reconstructed WIMP mass.

We also found that imposing a cut $Q_{\max}$ may actually be beneficial for small event samples. This is related to our earlier observation [14] that a typical experiment will under–estimate the higher moments of f_1, which receive significant contributions from recoil energies where only a fraction of an event is expected to occur in a given experiment. This problem becomes more acute for heavier target nuclei, since they have softer form factors. In particular, using Xenon rather than Germanium does not improve the determination of m_χ, since the spin–independent elastic form factor of Xenon as predicted by the Woods–Saxon ansatz vanishes for $Q \simeq 95$ keV. In contrast, the lower (threshold) energy of the experiment does not seem to be very important, if it can be pushed down to values near 3 keV or less.

Our analysis is idealized in that we ignore backgrounds, systematic uncertainties as well as the finite energy resolution. The relative error on the recoil energy in existing experiments is small compared to our most optimistic relative WIMP mass error estimates even with 500 events per experiment, so ignoring it should be a good approximation. Modern methods of discriminating between nuclear recoils and other events, combined with muon veto and good shielding, hold out the possibility of keeping (some) experiments nearly background–free also in future.

In our numerical analysis we have ignored the expected annual modulation of the WIMP flux. In practice this can be done if one simply sums all events over (at least) one full calendar

year. In principle one can also use our methods for subsets of data collected during specific times of the year. However, at least if the standard "shifted Gaussian" velocity distribution is approximately correct, we do not expect the small annual modulation to play a significant role, even if one compares experiments taken during different parts of the year.

We saw that our methods work best if the WIMP mass lies in between the masses of the two target nuclei. Even in that case the error will likely be significantly larger than the error on m_χ from collider experiments, if the WIMP is part of a well–motivated extension of the Standard Model of particle physics, e.g., if it is the lightest neutralino [6] or the lightest T−odd particle in "Little Higgs" models [18]. It will nevertheless be crucial to determine the WIMP mass from direct and/or indirect Dark Matter experiments as precisely as possible, in order to make sure that the particle produced at colliders is indeed the WIMP detected by these experiments. Once one is confident of this identification, one can use further collider measurements to constrain the WIMP couplings. This in turn will allow to calculate the WIMP–nucleus scattering cross section. Together with the determination of the WIMP velocity distribution [14], this will then yield a determination of the local WIMP number density via the total counting rate in direct detection experiments. Knowledge of the WIMP couplings will also permit prediction of the WIMP annihilation cross section. Together with the Dark Matter density inferred from cosmological observations, this will allow to test our understanding of the early universe [19]. A determination of the WIMP mass from Dark Matter detection experiments is thus a crucial ingredient in many analyses that shed light on the dark sector of the universe.

Acknowledgments

A Derivatives needed in the error analysis

At the end of Sec. 2 we gave the covariance matrix of the quantities appearing in the definition of the $\mathcal{R}_n$ as well as $\mathcal{R}_\sigma$. In Eqs.(46) and (49) we also gave expressions relating the errors on the reconstructed WIMP masses to the errors on $\mathcal{R}_n$ and $\mathcal{R}_\sigma$. The only missing ingredients in the calculation of the errors on our various estimators of m_χ are the first derivatives of $\mathcal{R}_n$ and $\mathcal{R}_\sigma$.

We begin with the former. From Eq.(45), it can be found directly that

$$
\frac{\partial \mathcal{R}_n}{\partial r_X(Q_{\min,X})} = \frac{2}{n} \left[\frac{Q_{\min,X}^{(n+1)/2} I_{0,X} - (n+1) Q_{\min,X}^{1/2} I_{n,X}}{2 Q_{\min,X}^{(n+1)/2} r_X(Q_{\min,X}) + (n+1) I_{n,X} F_X^2(Q_{\min,X})} \right]
$$
$$
\times \left[\frac{F_X^2(Q_{\min,X})}{2 Q_{\min,X}^{1/2} r_X(Q_{\min,X}) + I_{0,X} F_X^2(Q_{\min,X})} \right] \mathcal{R}_n, \qquad \text{(A1a)}
$$

$$
\frac{\partial \mathcal{R}_n}{\partial I_{n,X}} = \frac{n+1}{n} \left[\frac{F_X^2(Q_{\min,X})}{2 Q_{\min,X}^{(n+1)/2} r_X(Q_{\min,X}) + (n+1) I_{n,X} F_X^2(Q_{\min,X})} \right] \mathcal{R}_n,
$$
$$
\text{(A1b)}
$$

and

$$
\frac{\partial \mathcal{R}_n}{\partial I_{0,X}} = -\frac{1}{n} \left[\frac{F_X^2(Q_{\min,X})}{2 Q_{\min,X}^{1/2} r_X(Q_{\min,X}) + I_{0,X} F_X^2(Q_{\min,X})} \right] \mathcal{R}_n. \qquad \text{(A1c)}
$$

By first exchanging $Q_{\min,X}^{(n+1)/2}$ and $(n+1)I_{n,X}$ with $Q_{\min,X}^{1/2}$ and $I_{0,X}$, respectively, and then replacing X by Y, one finds

$$\frac{\partial \mathcal{R}_n}{\partial r_Y(Q_{\min,Y})} = -\frac{2}{n} \left[\frac{Q_{\min,Y}^{(n+1)/2} I_{0,Y} - (n+1)Q_{\min,Y}^{1/2} I_{n,Y}}{2Q_{\min,Y}^{(n+1)/2} r_Y(Q_{\min,Y}) + (n+1)I_{n,Y}F_Y^2(Q_{\min,Y})} \right]$$
$$\times \left[\frac{F_Y^2(Q_{\min,Y})}{2Q_{\min,Y}^{1/2} r_Y(Q_{\min,Y}) + I_{0,Y}F_Y^2(Q_{\min,Y})} \right] \mathcal{R}_n \,, \qquad (A2a)$$

$$\frac{\partial \mathcal{R}_n}{\partial I_{n,Y}} = -\frac{n+1}{n} \left[\frac{F_Y^2(Q_{\min,Y})}{2Q_{\min,Y}^{(n+1)/2} r_Y(Q_{\min,Y}) + (n+1)I_{n,Y}F_Y^2(Q_{\min,Y})} \right] \mathcal{R}_n \,, \qquad (A2b)$$

and

$$\frac{\partial \mathcal{R}_n}{\partial I_{0,Y}} = \frac{1}{n} \left[\frac{F_Y^2(Q_{\min,Y})}{2Q_{\min,y}^{1/2} r_Y(Q_{\min,Y}) + I_{0,Y}F_Y^2(Q_{\min,Y})} \right] \mathcal{R}_n \,. \qquad (A2c)$$

Note that a factor $\mathcal{R}_n$ appears in all these expressions; this allows to cast the final result for the error on m_χ estimated using moments of f_1 into a form analogous to that in Eq.(36) even in the presence of non–trivial cuts on the recoil energy, with the same prefactor. Moreover, all the $I_{0,X}$, $I_{0,Y}$, $I_{n,X}$, $I_{n,Y}$ should be understood to be computed according to Eq.(14) or its discretization (25) with integration limits $Q_{\min}$ and $Q_{\max}$ specific for that target.

Similarly, the derivatives of $\mathcal{R}_\sigma$ can be computed from Eq.(48):

$$\frac{\partial \mathcal{R}_\sigma}{\partial r_X(Q_{\min,X})} = \left[\frac{2Q_{\min,X}^{1/2}}{2Q_{\min,X}^{1/2} r_X(Q_{\min,X}) + I_{0,X}F_X^2(Q_{\min,X})} \right] \mathcal{R}_\sigma \,, \qquad (A3a)$$

and

$$\frac{\partial \mathcal{R}_\sigma}{\partial I_{0,X}} = \left[\frac{F_X^2(Q_{\min,X})}{2Q_{\min,X}^{1/2} r_X(Q_{\min,X}) + I_{0,X}F_X^2(Q_{\min,X})} \right] \mathcal{R}_\sigma \,, \qquad (A3b)$$

The derivatives with respect to the Y variables can be obtained from Eqs.(A3a) and (A3b) by simply changing $X \longrightarrow Y$ everywhere and changing the overall plus signs to minus signs.

References

[1] F. Zwicky, *Helv. Phys. Acta* **6**, 110 (1933); S. Smith, *Astrophys. J.* **83**, 23 (1936).

[2] V. C. Rubin and W. K. Ford, *Astrophys. J.* **159**, 379 (1970); S. M. Faber and J. S. Gallagher, *Annu. Rev. Astron. Astrophys.* **17**, 135 (1979); V. C. Rubin, W. K. Ford, and N. Thonnard, *Astrophys. J.* **238**, 471 (1980); K. G. Begeman, A. H. Broeils, and R. H. Sanders, *Mon. Not. R. Astron. Soc.* **249**, 523 (1991); R. P. Olling and M. R. Merrifield, *Mon. Not. R. Astron. Soc.* **311**, 361 (2000).

[3] M. Fich and S. Tremaine, *Annu. Rev. Astron. Astrophys.* **29**, 409 (1991).

[4] WMAP Collab., D. N. Spergel *et al.*, *Astrophys. J. Suppl.* **170**, 377 (2007).

[5] D. Clowe *et al.*, *Astrophys. J. Lett.* **648**, L109 (2006); D. Clowe, S. W. Randall, and M. Markevitch, *Nucl. Phys. Proc. Suppl.* **173**, 28 (2007).

[6] G. Jungman, M. Kamionkowski, and K. Griest, *Phys. Rep.* **267**, 195 (1996); G. Bertone, D. Hooper, and J. Silk, *Phys. Rep.* **405**, 279 (2005).

[7] M. W. Goodman and E. Witten, *Phys. Rev.* **D 31**, 3059 (1985); I. Wassermann, *Phys. Rev.* **D 33**, 2071 (1986); K. Griest, *Phys. Rev.* **D 38**, 2357 (1988); P. F. Smith and J. D. Lewin, Phys. Rep. **187**, (1990) 203.

[8] A. K. Drukier, K. Freese, and D. N. Spergel, *Phys. Rev.* **D 33**, 3495 (1986); K. Freese, J. Frieman, and A. Gould, *Phys. Rev.* **D 37**, 3388 (1988).

[9] A. M. Green, *J. Cosmol. Astropart. Phys.* **0708**, 022 (2007), `arXiv:hep-ph/0703217`.

[10] See e.g., A. Tasitsiomi, *Int. J. Mod. Phys.* **D 12**, 1157 (2003).

[11] M. Kamionkowski and A. Kinkhabwala, *Phys. Rev.* **D 57**, 3256 (1998).

[12] P. Sikivie and J. R. Ipser, *Phys. Lett.* **B 291**, 288 (1992); P. Sikivie, *Phys. Lett.* **B 567**, 1 (2003); A. Natarajan and P. Sikivie, *Phys. Rev.* **D 73**, 023510 (2006), and *Phys. Rev.* **D 76**, 023505 (2007), `arXiv:0705.0001 [astro-ph]`.

[13] K. Freese, P. Gondolo, H. J. Newberg, and M. Lewis, *Phys. Rev. Lett.* **92**, 111301 (2004).

[14] M. Drees and C. L. Shan, *J. Cosmol. Astropart. Phys.* **0706**, 011 (2007), `arXiv:astro-ph/0703651`.

[15] For a brief review on direct Dark Matter detection techniques, see the contribution by M. Drees and G. Gerbier to the Particle Data Booklet, W.-M. Yao *et al.*, *J. Phys.* **G 33**, 1 (2006).

[16] J. Engel, *Phys. Lett.* **B 264**, 114 (1991).

[17] H. T. Wong, `arXiv:0803.0033 [hep-ex]` (2008).

[18] See e.g., A. Birkedal, A. Noble, M. Perelstein, and A. Spray, *Phys. Rev.* **D 74**, 035002 (2006).

[19] See e.g., M. Drees, H. Iminniyaz, and M. Kakizaki, *Phys. Rev.* **D 76**, 103524 (2007), `arXiv:0704.1590 [hep-ph]`; D. J. H. Chung, L. L. Everett, K. Kong, and K. T. Matchev, *J. High Energy. Phys.* **0710**, 016 (2007), `arXiv:0706.2375 [hep-ph]`.